LAWRENCE
LIVERMORE
NATIONAL
LABORATORY

UCRL-JRNL-227164

Relativistic many-body calculations of electric-dipole lifetimes, rates, and oscillator strengths of Delta(n) = 0 transitions between 3l^-1 4l' states in Ni-like ions

U. I. Safronova, A. S. Safronova, P. Beiersdorfer

January 10, 2007

Journal of Physics B: Atomic, Molecular, and Optical Physics

This work was performed under the auspices of the U. S. Department of Energy by University of California, Lawrence Livermore National Laboratory under Contract W-7405-Eng-48.

Relativistic many-body calculations of electric-dipole lifetimes, rates, and oscillator strengths of $\Delta n = 0$ transitions between $3l^{-1}4l'$ states in Ni-like ions

U. I. Safronova, A. S. Safronova
Physics Department, University of Nevada, Reno, NV 89557

P. Beiersdorfer
Lawrence Livermore National Laboratory, Livermore, CA 94550

Transition rates, oscillator strengths, and line strengths are calculated for electric-dipole (E1) transitions between odd-parity $3s^23p^63d^94l_1$, $3s^23p^53d^{10}4l_2$, and $3s3p^63d^{10}4l_1$ states and even-parity $3s^23p^63d^94l_2$, $3s^23p^53d^{10}4l_1$, and $3s3p^63d^{10}4l_2$ (with $4l_1 = 4p, 4f$ and $4l_2 = 4s, 4d$) in Ni-like ions with the nuclear charges ranging from $Z = 34$ to 100. Relativistic many-body perturbation theory (RMBPT), including the Breit interaction, is used to evaluate retarded E1 matrix elements in length and velocity forms. The calculations start from a $1s^22s^22p^63s^23p^63d^{10}$ Dirac-Fock potential. First-order RMBPT is used to obtain intermediate coupling coefficients and second-order RMBPT is used to calculate transition matrix elements. Contributions from negative-energy states are included in the second-order E1 matrix elements to ensure the gauge independence of transition amplitudes. Transition energies used in the calculation of oscillator strengths and transition rates are from second-order RMBPT. Lifetimes of the $3s^23p^63d^94d$ levels are given for $Z = 34$–100. Transition rates, line strengths, and oscillator strengths are compared with critically evaluated experimental values and with results from other recent calculations. These atomic data are important in modeling of M-shell radiation spectra of heavy ions generated in electron beam ion trap experiments and in M-shell diagnostics of plasmas.

PACS numbers: 31.15.Ar, 31.15.Md, 32.70.Cs, 32.30.Rj, 31.25.Jf

I. INTRODUCTION

Recently multipole 3-4 transition wavelengths and rates between $3l^14l$ excited and ground states in nickel-like ions have been calculated using a relativistic many-body theory [1–4]. We continue this work to study atomic characteristics of the 4–4 and 3–3 transitions in nickel-like ions. The Ni-isoelectronic sequence has been studied extensively in connection with x-ray lasers [5–15]. Recently, an investigation into the use of atomic databases in simulation of Ni-like gadolinium x-ray laser was presented by King *et al.* in Ref. [16]. Several line-overlap measurements relevant to Ni-like x-ray lasers have also been performed [17–19]. In addition, x-ray spectral measurements of the line emission of $n = 3$–4, 3–5, 3–6, and 3–7 transitions in Ni- to Kr-like Au ions in electron beam ion trap (EBIT) plasma were reported by May *et al.* in Ref. [20]. X-ray spectra of Ni-like W including 3-4, 5, and 6 transitions recorded by a broadband microcalorimeter, were analyzed in Refs. [21, 22]. A detailed analysis of 3-4 and 3-5 transitions in the x-ray spectrum by laser produced plasmas of Ni-like highlycharged ions was presented by Doron *et al.* [23] (Ba^{28+}), by Zigler *et al.* [24] (La^{29+} and Pr^{31+}), by Doron *et al.* [25] (Ce^{30+}). Studies of Ni-like ions (Gd^{36+} and W^{46+}) have also been carried out on tokamaks [26, 27]. The spectrum of tungsten is expected to play an important role in tokamak diagnostics with the advent of the International Tokamak Engineering Reactor (ITER), which will use plasma facing components made of tungsten.

Various computer codes were employed to calculate transitions in Ni-like ions. In particular, ab-initio calculations were performed in Ref. [23] using the RELAC relativistic computer code to identify $3d - nf$ (n=4 to 8) transitions of Ni-like Ba. Atomic structure calculations for highly ionized tungsten (Co-like W^{47+} to Rb-like W^{37+}) were done by Fournier [28] with using the graphical angular momentum coupling code ANGULAR and the fully relativistic parametric potential code RELAC. The Hebrew University Lawrence Livermore Atomic Code HULLAC is also based on a relativistic model potential [29]. Ab-initio calculations with the HULLAC relativistic code was used for detailed analysis of spectral lines by Zigler *et al.* [24] and by May *et al.* in Ref. [20]. Zhang *et al.* [30], using the Dirac-Fock-Slater (DFS) code evaluated excitation energies and oscillator strengths of 3-4 and 3-5 transitions for the 33 Ni-like ions with $60 \leq Z \leq 92$. The multiconfiguration Dirac-Fock calculations of the $3d_{3/2} - 5f_{5/2}$, $3d_{5/2} - 5f_{7/2}$, $3d_{3/2} - 6f_{5/2}$, and $3d_{5/2} - 6f_{7/2}$ transitions were reported by Elliott *et al.* in Ref. [31]. The wavelengths and transition rates for $3l - nl'$ electric-dipole transitions in Ni-like xenon are presented by Skobelev *et al.* in Ref. [32]. Results were obtained by three methods: the relativistic Hartree-Fock (HFR) self-consistent-field method (Cowan code), multiconfiguration Dirac-Fock (MCDH) method (Grant code), and the HULLAC code. The contribution of lots of weak correlation on transition wavelengths and probabilities by including partly single and double excitation from the $3l$ inner-shells into the $4l$ and $5l$ orbital layers of highly-charged Ni-like ions were discussed by Dong *et al.* in Ref. [33]. Energy levels,

transition probabilities, and electron impact excitation for possible x-ray line emissions of Ni-like tantalum ions were recently calculated by Zhong *et al.* in Ref. [34]. Also, the overview of theoretical and experimental works on the $3l - nl'$ transitions in Ni-like ions can be found elsewhere (see, for example, Refs. [1–4] and references therein).

There are fewer studies of the $4s - 4p$ and $4p - 4d$ transitions in Ni-like ions [35–42]. Demonstration of soft-x ray amplification in nickel-like ions was reported by MacGowan *et al.* in Refs. [37–39]. The first observation of amplification of spontaneous emission at soft x-ray wavelengths by Eu^{35+} and Yb^{42+} ions was reported in 1987 [37]. The ions were created by high-intensity laser irradiation of a thin foil. Gains of order 1 cm^{-1} were observed on $J =$ 0-1, $4d-4p$ transitions in Eu^{35+}. The Ni-like $4d-4p$ laser scheme was extended later [38] to wavelengths near the K absorption edge of carbon. Gains of 2.3 cm^{-1} and 2.6 cm^{-1} were observed in Ni-like Ta^{45+} and W^{46+}, respectively. Identification of n =4, $\Delta n = 0$ transitions in the spectra of nickel-like ions from $Z = 37$ (Rb^{9+}) to $Z = 50$ (Sn^{22+}) was reported by Churilov *et al.* in Ref. [36]. The spectra were excited in the laser-produced plasma. Classification of the nickel-like silver and cadmium spectra (Ag^{19+} and Cd^{20+}) from a fast capillary discharge plasma was presented by Rahman *et al.* in Refs. [40, 41]. Fifty-three Cd XXI and forty-three Ag XX transitions ($3d^9 4p - 3d^9 4d$ and $3d^9 4d - 3d^9 4f$) were identified with the assistance of calculations performed using the Slater–Condon method with generalized least–squares fits of the energy parameters [40, 41]. Recently, the spectrum of nickel-like Kr IX excited in a fast capillary discharge and photographed with high resolution in the 300–800 Åwavelength region was investigated by Churilov *et al.* in Ref. [42]. The analysis was carried out on a basis of the energy parameters interpolation in the Ni I isoelectronic sequence. The 115 spectral lines in Kr^{8+} belonging to the $3d^9 4s - 3d^9 4p - 3d^9 4d - 3d^9 4f$ transitions were classified for the first time and the complete energy structures of the $3d^9 4s$, $3d^9 4p$, $3d^9 4d$, and $3d^9 4f$ configurations were presented. The experimental results were confirmed by the Generalized Least Squares (GLS) [42].

A comprehensive survey of M-shell transitions of Au and W produced on the LLNL electron beam ion trap (EBIT) was accomplished in [20–22]. Transitions $\Delta n = 0$ ($n = 4$) were not yet observed, such transitions though in EUV spectra from Rb- to Cu-like Au and W ions were already measured [43, 44]. Observation of the 4-4 transitions, however, appear feasible, and future measurements may include these transitions in Ni-like Au and W ions.

In the present paper, relativistic many-body perturbation theory (RMBPT) is used to determine matrix elements, oscillator strengths, and transition rates for allowed and forbidden electric-dipole transitions within the $3s^2 3p^6 3d^9 4l$, $3s^2 3p^5 3d^{10} 4l$, and $3s 3p^6 3d^{10} 4l$ complexes of states in Ni-like ions with nuclear charges ranging from $Z = 34$ to 100. Retarded E1 matrix elements are evaluated in both length and velocity forms. These calculations start from a $1s^2 2s^2 2p^6 3s^2 3p^6 3d^{10}$ Dirac-Fock potential. First-order perturbation theory is used to obtain intermediate coupling coefficients and second-order RMBPT is used to determine transition matrix elements. Contributions from negative-energy states are included in the second-order E1 matrix elements to ensure an agreement between the length-form and velocity-form amplitudes. The transition energies used in the calculation of oscillator strengths and transition rates are obtained from the second-order RMBPT. Lifetimes of the $3s^2 3p^6 3d^9 4d$ levels are given for $Z = 34$–100.

In summary, this work presents both a systematic calculation of the transition probabilities between excited states in Ni-like ions and a study of the importance of the correlation corrections to those properties. The final results are used to calculate lifetimes of levels and to provide benchmark values for Ni-like ions. Our data are compared with the existing measurements.

II. METHOD

In this section, we write down and discuss the relativistic MBPT formulas for first- and second-order matrix elements for transitions between excited states in atomic systems with one hole in the closed shells and one electron above the closed shells. We consider the coupled states $\Phi_{JM}(a^{-1}v)$ defined by

$$\Phi_{JM}(a^{-1}v) = \sqrt{2J+1} \sum_{m_a m_v} (-1)^{j_v - m_v} \begin{pmatrix} j_v & J & j_a \\ -m_v & M & m_a \end{pmatrix} a^\dagger_{v m_v} a_{a m_a} |0\rangle \,, \tag{1}$$

where $|0\rangle$ is the closed-shell ground state, the single-particle index v designates the valence state and the single-hole indices a range over the closed core. Below, we use both jj and LS designations for hole-particle states. Instead of using the $a^{-1}v$ designations, we use simpler designations av in all following tables and in the text below.

The first-order reduced electric-dipole matrix element $Z^{(1)}$ for the transition between the hole-particle states $av(J)$–$cw(J')$ is given by

$$\begin{aligned} Z^{(1)}(av(J), cw(J')) \;=\; & \sqrt{[J][J']} \Bigg[\delta(c,a) Z(wv) (-1)^{j_v + j_c + 1 + J'} \begin{Bmatrix} J & J' & 1 \\ j_w & j_v & j_a \end{Bmatrix} \\ & + \delta(w,v) Z(ac) (-1)^{j_v + j_c + J + 1} \begin{Bmatrix} J & J' & 1 \\ j_c & j_a & j_v \end{Bmatrix} \Bigg] , \end{aligned} \tag{2}$$

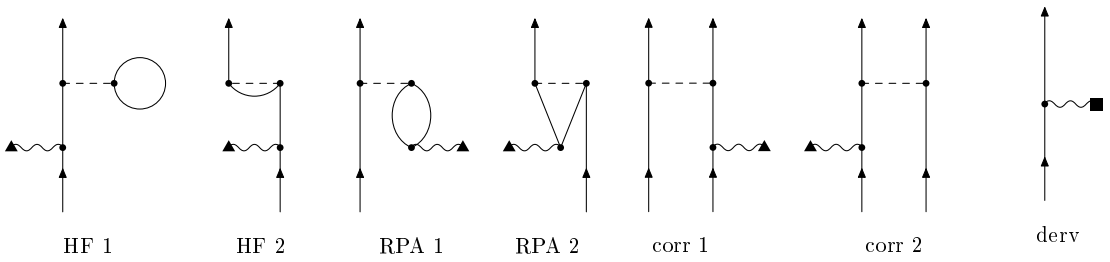

FIG. 1: Second-order diagrams for electric-dipole matrix elements.

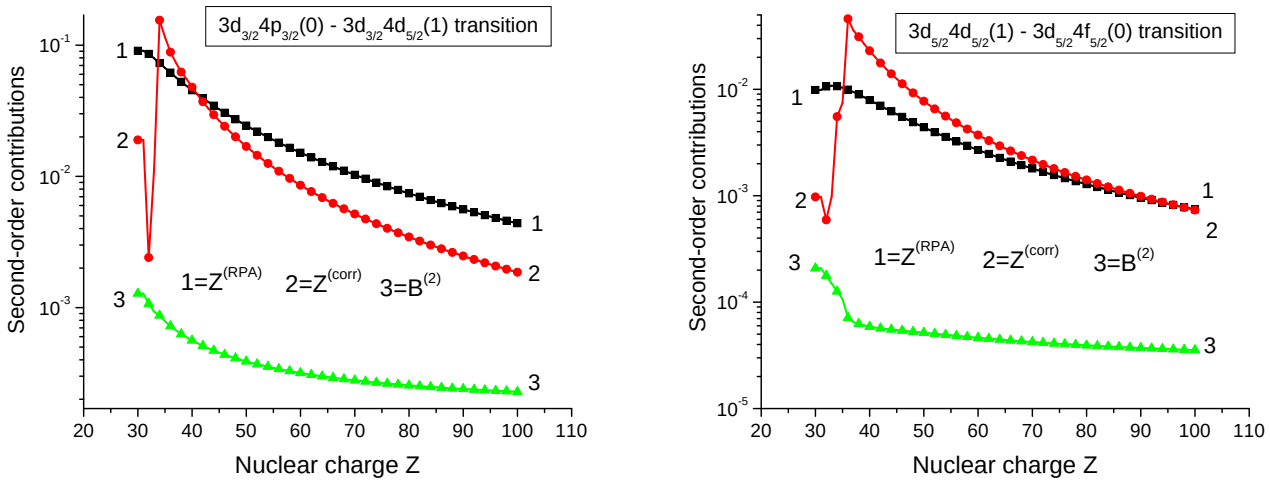

FIG. 2: Second-order contributions for electric-dipole matrix elements in Ni-like ions as functions of Z.

where $[J] = 2J + 1$. The dipole matrix elements $Z(vw)$, that include retardation, are given in velocity and length forms by Eqs.(3,4) of Ref. [45].

The second-order reduced matrix element $Z^{(2)}$ for the transition between the hole-particle states $av(J)$–$cw(J')$ consists of four contributions: Dirac-Hartree-Fock (HF) term ($Z^{(\mathrm{HF})}$), random-phase approximation (RPA) term ($Z^{(\mathrm{RPA})}$), correlation contribution (corr) term ($Z^{(\mathrm{orr})}$), and derivative (derv) term, $Z^{(\mathrm{derv})}$. The "HF", "RPA", "corr", and "derv" contributions in second-order matrix elements in terms of Bruckner-Golstone diagrams are illustrated in Fig. 1. The dashed lines designate Coulomb + Breit interactions and the wavy lines designate interactions with the dipole field. Diagrams "HF 1" and "HF 2" as well as diagrams "RPA 1" and "RPA 2" are direct and exchange contributions. These diagrams account for the shielding of the dipole field by the core electrons. Diagrams "corr 1" and "corr 2" are direct and exchange correlation contributions. These diagrams correct the matrix element to account for interaction between the valence electrons. The "derv" diagram represents symbolically the second-order RMBPT correction from the derivative term [1]. A detailed discussion of these diagrams for systems with two valence electrons was given by Safronova *et al.* in Ref. [46]. Analytical expressions for the second-order contributions $Z^{(\mathrm{DF})}$, $Z^{(\mathrm{RPA})}$, $Z^{(\mathrm{corr})}$, and $Z^{(\mathrm{derv})}$ for transitions between excited states in hole-particle systems were presented recently [47].

All of the second-order correlation corrections that we discussed above result from the residual Coulomb interaction. To include correlation corrections due to the Breit interaction, the Coulomb matrix element $X_k(abcd)$ must be modified according to the rule

$$X_k(abcd) \to X_k(abcd) + M_k(abcd) + N_k(abcd), \tag{3}$$

where M_k and N_k are magnetic radial integrals defined by Eqs.(A4,A5) in Ref. [48].

A. Uncoupled Matrix Elements

In Table I, we list values of the first- and second-order contributions to electric-dipole matrix elements $Z^{(\mathrm{DF})}$, $Z^{(\mathrm{RPA})}$, $Z^{(\mathrm{corr})}$, and the matrix element of the derivative term $P^{(\mathrm{derv})}$ for the odd-even $av(J) - a'v'(J')$ transitions with $J = 1$ and $J' = 0$, 1, 2 in Ni-like tungsten , Z=74. Both length and velocity forms of the matrix elements are given. The Coulomb second-order "HF" contribution $Z^{(\mathrm{HF})}$ vanishes in the present calculation since we use DF basis functions. We use the symbol B in Table I to denote the Coulomb-Breit contributions to the second-order matrix elements, and we tabulate $B^{(\mathrm{HF})}$, $B^{(\mathrm{RPA})}$, $B^{(\mathrm{corr})}$, and the totals $B^{(2)}$. The first-order contributions $Z^{(\mathrm{DF})}$ are different in length and velocity forms. Also the total second-order Breit corrections $B^{(2)}$ are smaller than the correlation corrections $Z^{(\mathrm{corr})}$ and these correlation contributions are smaller than the RPA terms $Z^{(\mathrm{RPA})}$. The ratios between these terms change with a nuclear charge as illustrated by Fig. 2 where second-order contributions $Z^{(\mathrm{RPA})}$, $Z^{(\mathrm{corr})}$, and $B^{(2)}$ are shown as functions of Z for the electric-dipole matrix elements $3d_{3/2}4p_{3/2}(0) - 3d_{3/2}4d_{5/2}(1)$ and $3d_{5/2}4d_{3/2}(1) - 3d_{5/2}4f_{5/2}(0)$. It should be noted that only the $Z^{(\mathrm{corr})}$ terms are non-zero for two-particle transitions such as the $3p_{1/2}4p_{1/2}(1) - 3p_{3/2}4d_{3/2}(0)$ transition. The values of $Z^{(\mathrm{corr})}$ terms for two-particle transitions are of the same order of magnitude as for the one-particle transitions (for example, $3p_{3/2}4d_{3/2}(1) - 3d_{3/2}4d_{5/2}(1)$ and $3p_{3/2}4d_{3/2}(1) - 3d_{3/2}4d_{3/2}(1)$ transitions).

B. Coupled Matrix Elements

As mentioned above, physical hole-particle states are the linear combinations of uncoupled hole-particle states. For the W^{46+} example discussed above, the transition amplitudes between physical states are the linear combinations of the uncoupled transition matrix elements given in Table I. The mixing coefficients and energies are obtained by diagonalizing the first-order effective Hamiltonian which includes both Coulomb and Breit interactions. We let $C_1^{\lambda}(av)$ designate the λ-th eigenvector of the first-order effective Hamiltonian and let E_1^{λ} be the corresponding eigenvalue. The coupled transition matrix element between the initial eigenstate I with the angular momentum J and the final state F with the angular momentum J' is given by:

$$
\begin{aligned}
Q^{(1+2)}(I-F) = {} & \frac{1}{E_1^I - E_1^F} \sum_{av} \sum_{cw} C_1^I(av) C_1^F(cw) \\
& \times \Big\{ [\varepsilon_{av} - \varepsilon_{cw}] \left[Z_1^{(1+2)}[av(J) - cw(J')] + B_1^{(2)}[av(J) - cw(J')] \right] \\
& + \left[E_1^I - E_1^F - \varepsilon_{av} + \varepsilon_{cw} \right] P_1^{(\mathrm{derv})}[av(J) - cw(J')] \Big\} . \qquad (4)
\end{aligned}
$$

Here, $\varepsilon_{av} = -\varepsilon_a + \varepsilon_v$ and $Z_1^{(1+2)} = Z^{(\mathrm{DF})} + Z^{(\mathrm{RPA})} + Z^{(\mathrm{corr})}$, and $B_1^{(2)} = B^{(\mathrm{HF})} + B^{(\mathrm{RPA})} + B^{(\mathrm{corr})}$. Using these formulas together with the uncoupled reduced matrix elements given in Table I, we transform the uncoupled matrix elements to matrix elements between coupled (physical) states.

Values of *coupled* reduced matrix elements in length and velocity forms are given in Table II for the transitions considered in Table I. Although we use an intermediate-coupling scheme, it is nevertheless convenient to label the physical states using the LS scheme. Both designations are given in Table II. We see that L and V forms of the coupled matrix elements in Table II differ only in the third or fourth digits. These L–V differences arise because we start our RMBPT calculations using a non-local Dirac-Fock (DF) potential. If we were to replace the DF potential by a local potential, the differences would disappear completely. The first two columns in Table II show L and V values of *coupled* reduced matrix elements calculated without the second-order contribution. As we see from this table, removing the second-order contribution increases the $L - V$ differences.

It should be emphasized that we include negative energy state (NES) contributions into the sums over the intermediate states. Ignoring the NES contributions leads only to small changes in the L-form matrix elements but to substantial changes in some of the V-form matrix elements, with a consequent loss of gauge independence for a local potential.

C. Negative-energy contributions

The NES contributions to the second-order reduced matrix elements arise from the terms in the sums over states i and n in the $Z^{(\mathrm{corr})}$ contributions [47]) for which $\varepsilon_i < -mc^2$. The NES contributions for non-relativistically allowed transitions were discussed in [3] for Ni-like ions, where they were found to be the most important for velocity-form matrix elements; they do not significantly modify length-form matrix elements. In Ref. [45], it was shown that NES

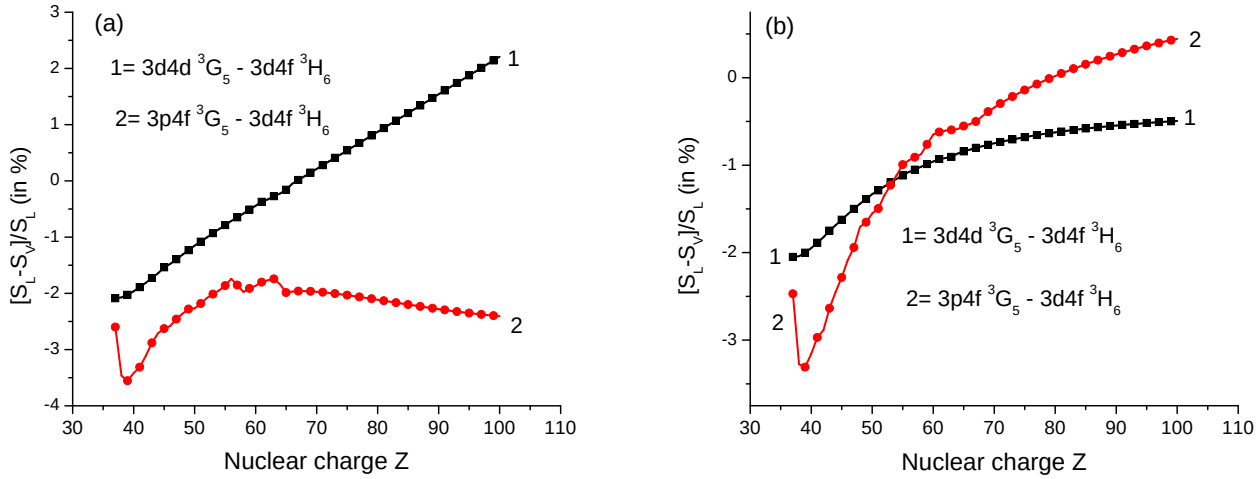

FIG. 3: Difference between the values of line strengths calculated in length (S_L) and velocity (S_V) gauges for E1 transitions in Ni-like ions as functions of Z. Graph (a) shows data without NES contributions and graph (b) shows data with NES contributions.

contributions can be of the same order of magnitude as the "regular" positive-energy contributions for certain non-relativistically forbidden transitions in Be-like ions. We observe similar large contributions here for LS-forbidden transitions. The matrix elements in Tables I and II include NES contributions.

In Fig. 3, we illustrate the Z-dependence of the differences between line strengths calculated in length S_L and velocity S_V forms for the $3d4d\ ^3G_5 - 3d4f\ ^3H_6$ and $3p4f\ ^3G_5 - 3d4f\ ^3H_6$ transitions. We plot the ratio $(S_L - S_V)/S_L$ (in percent) calculated without (a) and with (b) negative-energy state contributions to the second-order reduced matrix elements. The ratio $(S_L - S_V)/S_L$ for the $3d4d\ ^3G_5 - 3d4f\ ^3H_6$ transition decreases from 2% to 1% for Z = 34 up to Z = 100. The ratio $(S_L - S_V)/S_L$ decreases substantially (from 3% to 0% for high Z) when NES are included for the $3p4f\ ^3G_5 - 3d4f\ ^3H_6$ transition.

In view of the gauge dependence issue discussed above, our results below are presented in L form to decrease the volume of tabulate material. Uncertainties in the recommended values given in [49] were estimated to be less than 10% based on comparisons with experimental results from lifetime and emission measurements. The agreement between theoretical L-form and V-form results was also used in [49] as an indicator of accuracy. Since the present transition data are obtained using a single method for all Z, and improve in accuracy with increasing Z, we expect our data for high Z to be very reliable.

III. RESULTS AND DISCUSSION

We calculate line strengths, oscillator strengths, and transition probabilities for 1549 $[3l_14l_2\ ^{1,3}L_J - 3l_34l_4\ ^{1,3}L'_{J'}]$ lines for all ions with Z = 32–100. The results were calculated in both length and velocity forms but, since the L form is less sensitive to various contributions, only length-form results are presented in the following tables and figures. The theoretical energies used to evaluate oscillator strengths and transition probabilities are calculated using the second-order RMBPT formalism developed in Ref. [1].

A. Transition rates

The general trends of the Z-dependence of transition rates for the $3l_14l_2\ ^{1,3}L_J - 3l_34l_4\ ^{1,3}L'_{J'}$ lines are presented in Figs.4 and 5. Each figure in Fig.4 shows transitions to a fixed J state from states belonging to a limited set of states $3l4l'\ ^{1,3}L_J$, i.e. a *complex* of states. A complex includes all states of the same parity and J obtained from the combinations of the $3l4l'\ ^{1,3}L_J$ states. For example, the odd-parity complex with J=1 includes the states $3s4p\ ^{1,3}P_1$, $3p4s\ ^{1,3}P_1$, $3p4d\ ^3D_1$, $3p4d\ ^{1,3}P_1$, $3d4p\ ^3D_1$, $3d4p\ ^{1,3}P_1$, $3d4f\ ^3D_1$, and $3d4f\ ^{1,3}P_1$ in LS coupling or $3s4p_{1/2}[1]$, $3s4p_{3/2}[1]$, $3p_{1/2}4s[1]$, $3p_{3/2}4s[1]$, $3p_{1/2}4d_{3/2}[1]$, $3p_{3/2}4d_{3/2}[1]$, $3p_{3/2}4d_{5/2}[1]$, $3d_{3/2}4p_{1/2}[1]$, $3d_{3/2}4p_{3/2}[1]$,

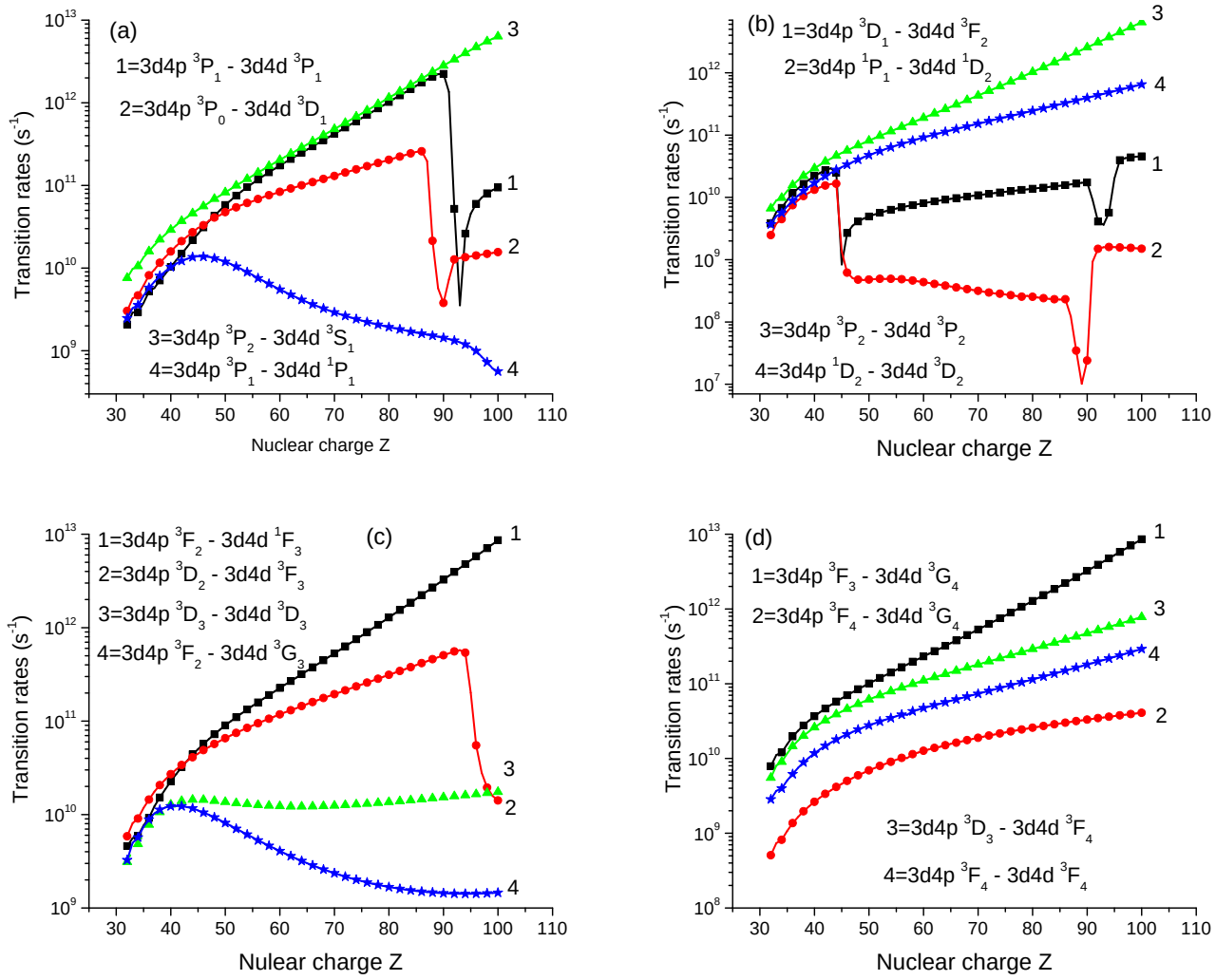

FIG. 4: Transition rates for odd-even transitions in Ni-like ions as function of Z.

$3d_{5/2}4p_{3/2}[1]$, $3d_{3/2}4f_{5/2}[1]$, $3d_{5/2}4f_{5/2}[1]$, and $3d_{5/2}4f_{7/2}[1]$ in jj coupling. Later, we use the LS designations since they are more conventional.

In Figs. 4a - Fig. 4d, we present a limited set (16 among 123) of transition probabilities for the $3d4p-3d4d$ lines. The $3d4p-3d4d$ transitions are illustrated by $3d4p\ ^{1,3}P_J-3d4d\ ^{1,3}L_1$, $3d4p\ ^{1,3}L'_J-3d4d\ ^{1,3}L_2$, $3d4p\ ^{1,3}L'_J-3d4d\ ^{1,3}L_3$, $3d4p\ ^3L'_J-3d4d\ ^3L_4$ transitions transitions shown in Figs. 4a, 4b, 4c and 4d, respectively.

In Figs. 5a and 5b, we present a limited set (8 among 36) of transition rates for the $3d4s-3d4p$ lines. The eight $3d4d-3d4f$ transitions (among 171 transitions) are presented in Figs. 5c and 5d. Transition rates for the two $3d4s\ ^{1,3}D_{J'}-3d4f\ ^{1,3}L_J$ lines (among 42 lines) are shown in Fig. 5c. It should be noted that all transitions shown in Figs. 4 and 5 are the allowed one-particle ($4p-4d$ transitions in Figs. 4 and $4s-4p$, $4d-4f$ transitions in Figs. 5), except two transitions shown in Fig. 5c. The latter ones are the $4s-4f$ transitions to be forbidden as dipole-electric one-particle transitions. The value of transition rates for these transitions are not zero because of two-particle interactions; between the $[3d4s+3d4d+3s4s]$ and $[3d4f+3d4p+3s4f]$ configurations as well as because of the second-order contribution from correlation diagrams ($Z^{\rm corr}(3d_{5/2}4s_{1/2}(2)-3d_{5/2}4f_{5/2}(1))=0.842874\times10^{-4}$ and $Z^{\rm corr}(3d_{3/2}4s_{1/2}(2)-3d_{5/2}4f_{5/2}(1))=$ -0.131785$\times10^{-3}$). We can see from Fig. 5c, that the transition rates of these two-particle $3d4s\ ^{1,3}D_{J'}-3d4f\ ^{1,3}L_J$ lines are smaller (by 2-4 orders of magnitude) than the transition rates of one-particle $3d4d\ ^3D_{J'}-3d4f\ ^3D_J$ lines for small Z but become even larger for high Z.

We see from the graphs that transitions with smooth Z dependencies are rarer than transitions with sharp features but still occur for all transition types: triplet-triplet, singlet-singlet, and singlet-triplet, and include transitions with both small J and large J. One general conclusion that can be derived from those graphs is that the smooth Z-

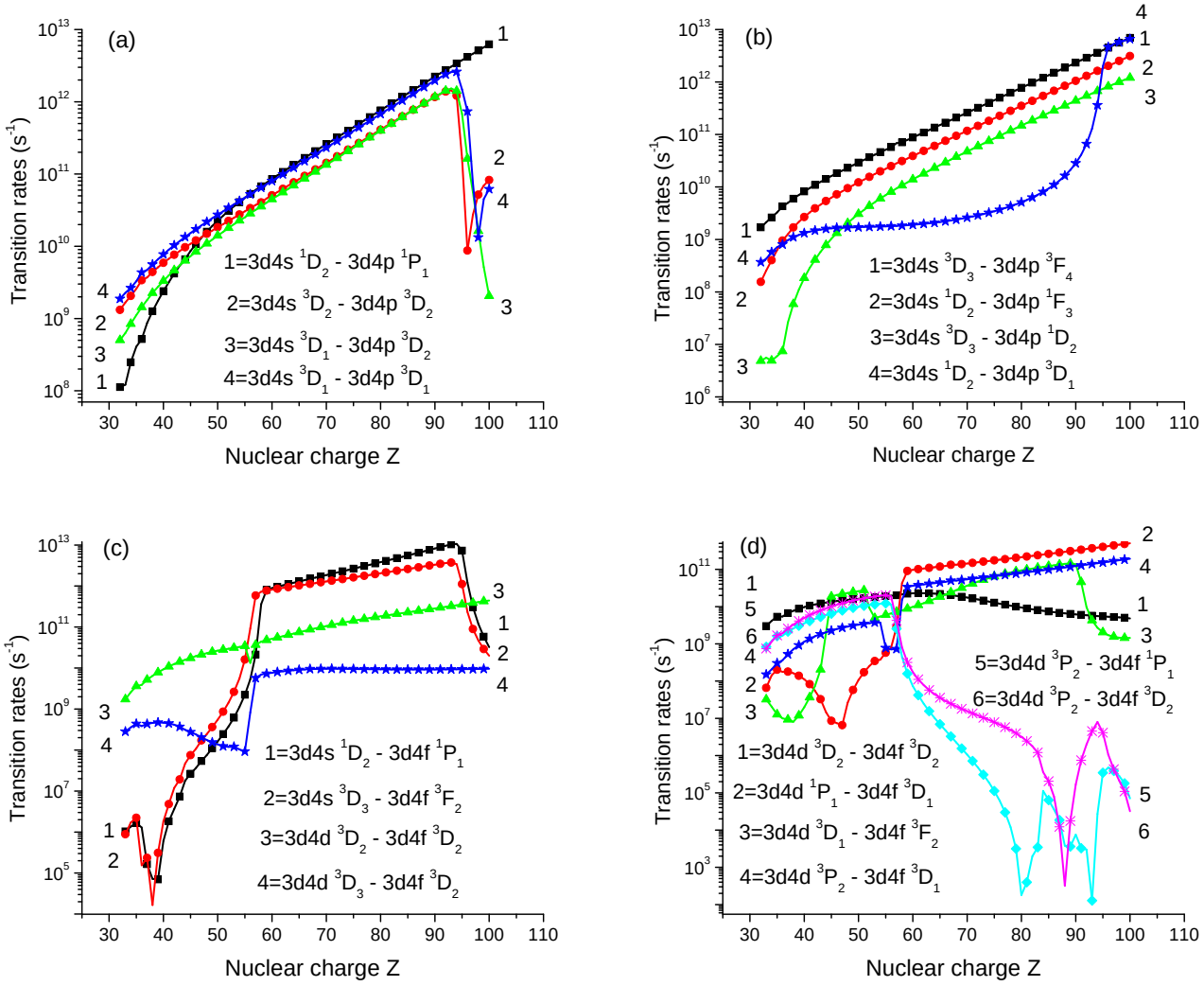

FIG. 5: Transition rates for even-odd transitions in Ni-like ions as function of Z.

dependences occur more frequently for transitions with the largest values of transition rates among the transitions inside complexes.

Singularities in the transition-rate curves have three distinct origins: avoided level crossings, zeros in the dipole matrix elements, and zeros in transition energies. Avoided level crossings result in changes of the dominant level configuration at a particular value of Z and lead to abrupt changes in the transition rate curves when the partial rates associated with the dominant configurations below and above the crossing point are significantly different. Zeros in transition matrix elements as functions of Z lead to cusp-like minima in the transition rate curves. Zeros in transition energies, occurring at high Z listed in Table III, also result in cusp-like minima in the transition rate curves. Examples of each of these three singularity types can be seen in Figs. 4 and 5. Dramatic examples of the first type, avoided level crossings, are seen in Fig. 4a at Z=90, corresponding to a change in the dominant configuration for the $3d4d\ ^3D_1$ state, the $3p_{3/2}4p_{1/2}(1)$ instead of the $3d_{3/2}4d_{3/2}(1)$ configuration. An avoided level crossing also occurs for the $3d4p\ ^3P_1 - 3d4d\ ^3P_1$ transition Fig. 4a at Z=93. Examples of the second type, zeros in matrix elements, are seen in Fig. 5d at Z=45-46 for the $3d4d\ ^1P_1 - 3d4f\ ^3D_1$ transition and at Z=55-56 for the $3d4d\ ^3D_1 - 3d4f\ ^3F_2$ transition. Finally, singularities of the third type, corresponding to an energy of almost zero are seen at Z= 88 for the transition in $3d4d\ ^3P_2 - 3d4f\ ^3D_2$ in Fig. 5d and at Z=80 and 93 for the $3d4d\ ^3P_2 - 3d4f\ ^1P_1$ transition in Fig. 5d. For both cases the inversion of levels involved in transitions occurs as demonstrated in Table III ($3d4d\ ^3P_2$, $3d4f\ ^3D_2$ levels and $3d4d\ ^3P_2$, $3d4f\ ^1P_1$ levels).

B. Wavelengths and transition rates

In Table IV, wavelengths and electric-dipole transition rates for $3d4p - 3d4d$ transitions in Ni-like Kr are presented. We limit the table to the transitions given in Ref. [42]. To avoid level identification problems, we present the LS and jj labels of the transitions and include both wavelengths and transition rates in Tables IV. We note that only the transitions with the largest values of A were experimentally observed. It should be noted that we arrange the data in groups with a fixed LSJ level of the upper state. We see from the comparison of RMBPT and experimental data in Table IV, that the agreement in wavelengths is about 0.1%–0.5%. It should be noted that the accuracy of the second-order RMBPT method increases with increasing a nuclear charge.

Transition rates in [42] were calculated in the Racah-Slater formalism by means of the RCN, RCG Cowan computer codes [50], using scaled Hartree-Fock (HF) integrals as initial parameters. The sets of the even $3d^{10}$, $3d^9ns$ (n = 4-6), $3d^9nd$ (n = 4-6), $3d^84s^2$, $3d^84s4d$, $3p^53d^{10}4p$, and $3p^53d^{10}4f$ configurations and the odd $3d^9np$ (n = 4-6), $3d^9nf$ (n = 4-6), $3d^84s4p$, $3d^84s4f$, and $3p^53d^{10}4s$, $3p^53d^{10}4d$ configurations have been used in these calculations. Highly excited configurations have been included as they have large integrals of interaction with the analyzed $3d^94l$ configurations [42]. The second-order RMBPT calculation includes partial waves up to $l_{\max} = 8$ and is extrapolated to account for contributions from higher partial waves. We use B-spline methods [51] to generate a complete set of basis DF wave functions for use in the evaluation of RMBPT expressions. For Ni-like ions, we use 50 splines of order $k = 8$ for each angular momentum. In Table IV, the RMBPT transition rates (gA_r) are compared with results given by Churilov *et al.* in Ref. [42]. The difference is about 10% for many transitions. This difference can be explained by contribution of highly excited states that could not be taken into account by the RCN, RCG Cowan computer codes [50].

In Table V, wavelengths and electric-dipole transition rates are presented for $3d4s - 3d4p$ transitions in Ni-like Pd^{18+}. The RMBPT results are compared with experimental measurements by Churilov *et al.* from Ref. [36]. We can see from Table V that our wavelengths results are in excellent agreement (0.04% – 0.2%) with experimental measurements. Our weighted transition rates for $3d4s - 3d4p$ transitions are compared with relative intensities given in [36]. In some cases the gA values are proportional relative intensities, however, we need additional calculations to build synthetic spectra to make comparison with relative intensities.

In Table VI, wavelengths (λ in $\mathring{A}$) and transition rates (gA in $10^{10}\mathrm{s}^{-1}$) are shown for the four $3d4p - 3d4d$ transitions in Ni-like ions. The RMBPT results are compared with experimental measurements by MacGowan *et al.* from Refs. [37, 38]. Experimental measurements for Ni-like Eu^{35+} and Yb^{42+} ions were reported in [37], however, the wavelengths data for Ta^{45+} and W^{46+} are from Ref. [38]. Our values of wavelengths for the $3d_{5/2}4p_{3/2}$ (1) $- 3d_{5/2}4d_{5/2}$ (1) and $3d_{5/2}4p_{3/2}$ (1) $- 3d_{5/2}4d_{5/2}$ (2) transitions is in a good agreement within the experimental uncertainty of the measurements in Ref. [37, 38], however, there is less agreement for the wavelengths of the $3d_{5/2}4p_{3/2}$ (1) $- 3d_{3/2}4d_{3/2}$ (0) and $3d_{3/2}4p_{1/2}$ (1) $- 3d_{3/2}4d_{3/2}$ (0) transitions (the difference is a factor of 2-4 of the experimental uncertainty). We did not find any data in [37, 38] to compare our RMBPT values of weighted transition rates given in the last column of Table VI.

C. Lifetimes data

In Table VII, we present a limited set (18 among 105) of our RMBPT lifetime data for the $3d4d$ LSJ levels in Ni-like ions with Z = 36–92. To avoid level identification problems, we present the LS and jj labels of the transitions and include both wavelengths and transition rates in Table VII. We can see from this table that for ions with Z = 36–50 there are rather small differences (about 10–20%) in lifetimes of the individual levels, except the $3d4d\ ^1S_0$ level. The difference increases for high-Z ions. For example, the the ratio of largest and smallest values of lifetime given in Table VII is equal to 1.9, 3.2, and 7.8 for ions with Z = 36, 54, and 92, respectively.

Results of the present calculation of the lifetimes are obtained by taking into account E1 transition rates from each upper level to all possible lower levels. The contributions of the different channels to the lifetimes of the $3d4d\ ^{1,3}L_J$ levels with J = 0–3 are shown in Figs. 6 and 7. The curves represent the ratios of individual transition probabilities A to the sum of all transition probabilities $\sum A$ for the level considered. As we see from the two upper panels of Fig. 6, the largest contribution to the lifetimes of the $3d4d\ ^3P_1$ level comes from the $3d4p\ ^3P_1$ state for low-Z ions and from $3d4p\ ^1P_1$ state for high-Z ions. We have opposite the situation for the $3d4d\ ^1S_0$ level; the $3d4p\ ^1P_1$ state gives the largest contribution for low-Z ions and the $3d4p\ ^3P_1$ state gives the largest contribution for high-Z ions.

Only for two levels presented in Figs. 6 and 7, the dominant transition does not change for the entire range of Z; the $3d4p\ ^3P_2 - 3d4d\ ^3S_1$ transition (the center left panel of Figs. 6) and the $3d4p\ ^1D_2 - 3d4d\ ^3D_2$ transition (the upper left panel of Fig. 7). The contribution of the dominant transition is 80%–90% in the first case (the $3d4d\ ^3S_1$ level), however, the contribution of the dominant transition for the $3d4d\ ^3D_2$ level is only 40%–60%.

For low-Z ions it is difficult to determine the dominant transition. Three transitions ($3d4p\ ^3P_0 - 3d4d\ ^3D_1$, $3d4p\ ^1P_1 - 3d4d\ ^3D_1$, and $3d4p\ ^3D_1 - 3d4d\ ^3D_1$) have almost equal contribution (20%–40%) to the lifetime of the

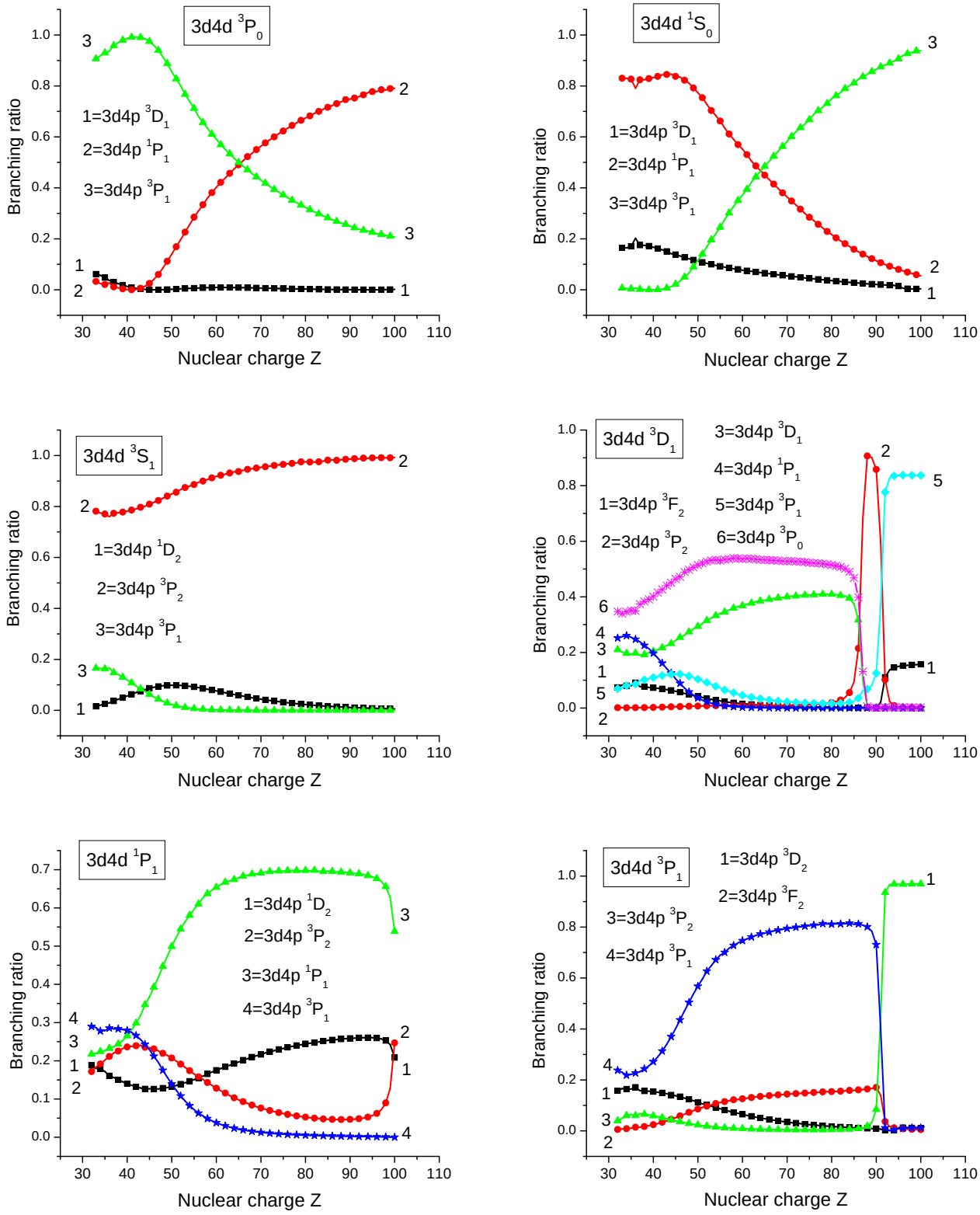

FIG. 6: Channel contributions to the lifetimes of the $3d4d\ ^{1,3}L_J$ ($J = 0, 1$) states.

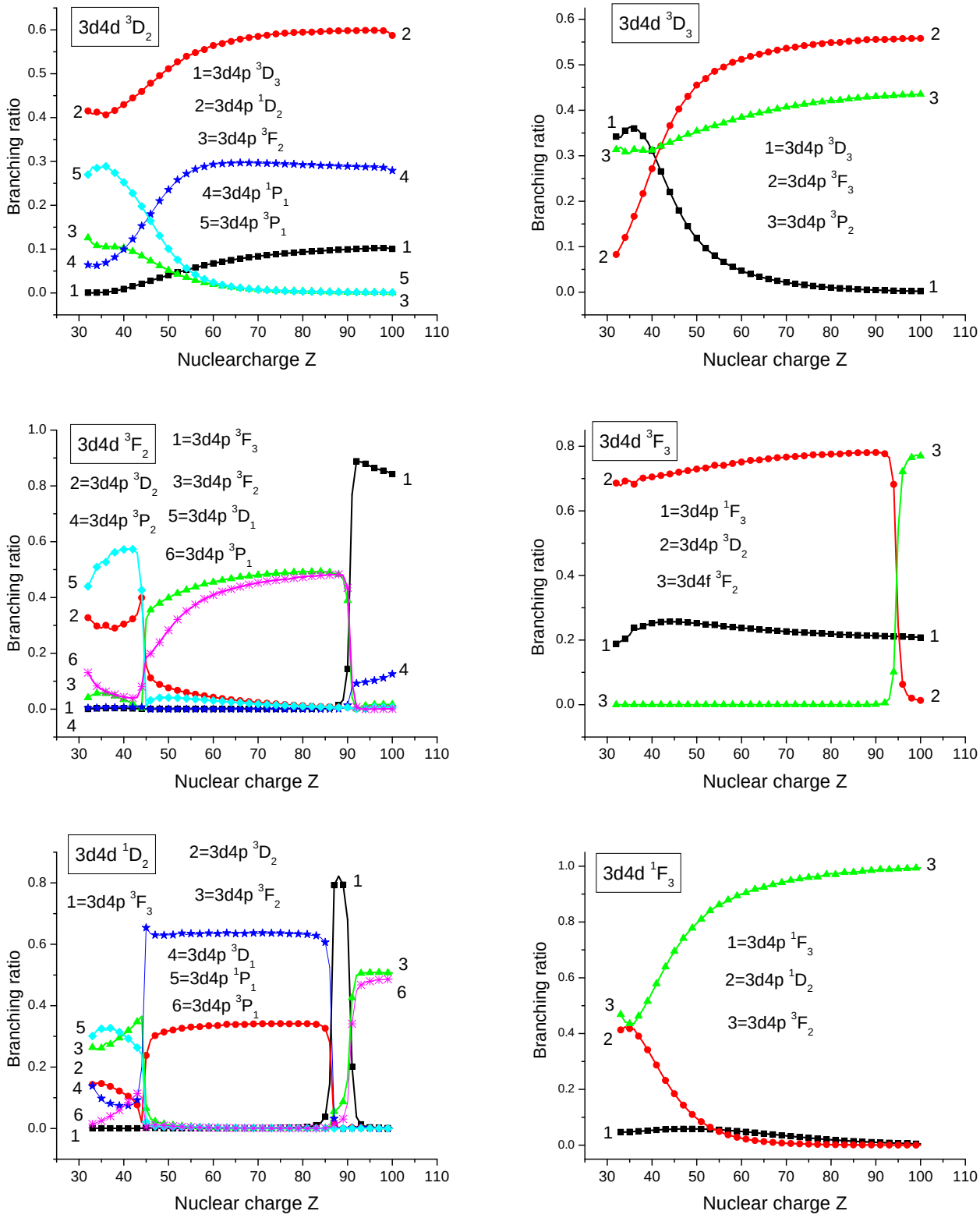

FIG. 7: Channel contributions to the lifetimes of the the $3d4d\ ^{1,3}L_J$ ($J = 2, 3$) states.

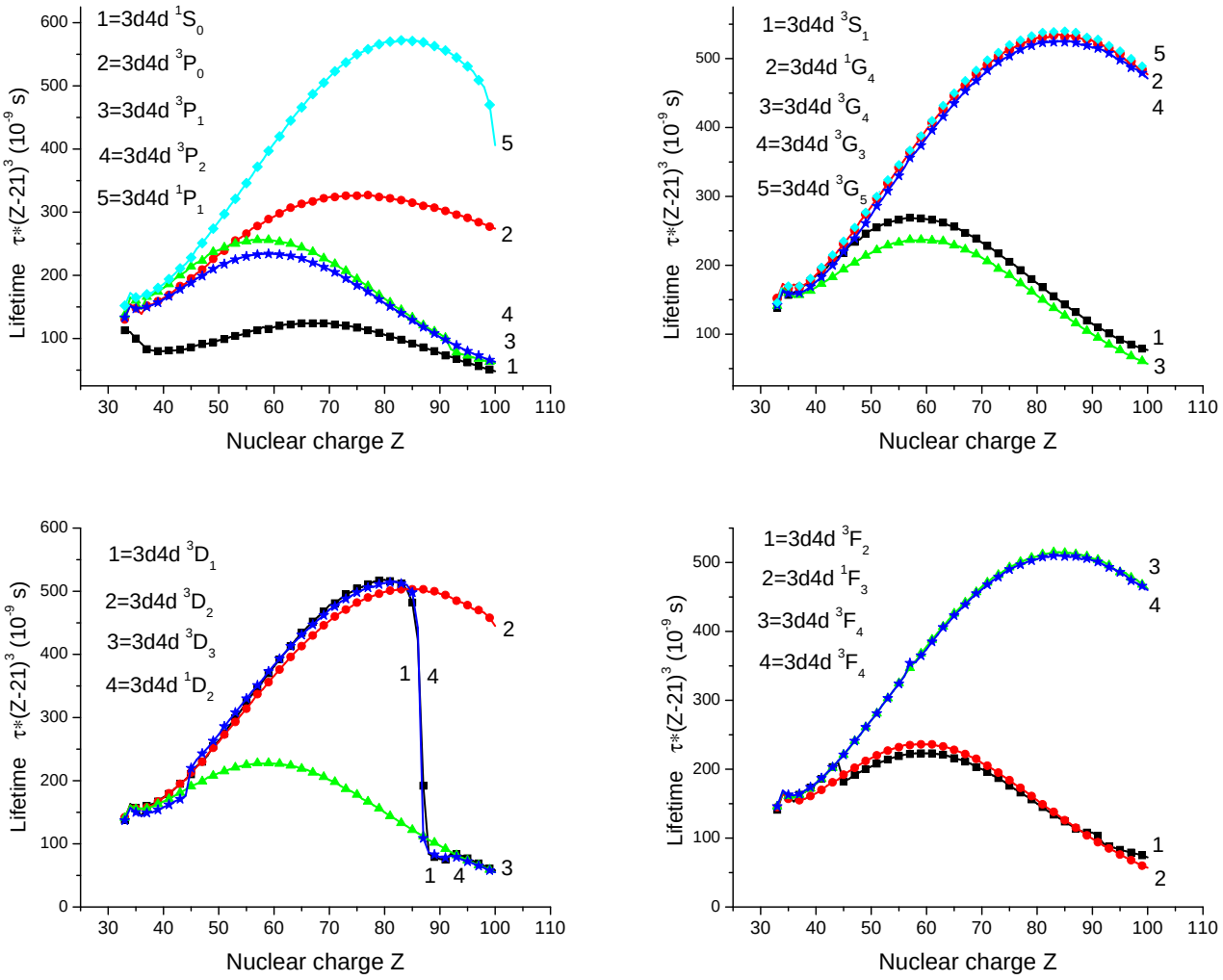

FIG. 8: Lifetimes $(\tau \times (Z-21)^3)$ of the $3d4d\ ^{1,3}L_J$ levels as function of Z in 10^{-9} s.

$3d4d\ ^3D_1$ level shown in the the center right panel of Fig. 6). A similar behavior of the branching ratios for the lifetimes of the $3d4d\ ^{1,3}P_1$ levels is seen on the two bottom panels of Fig. 6. Two transitions ($3d4p\ ^3D_3 - 3d4d\ ^3D_3$, and $3d4p\ ^3P_2 - 3d4d\ ^3D_3$) give the dominant and almost equal (30%–35%) contributions to the lifetime of the $3d4d\ ^3D_3$ level for the low-Z ions with Z =32–40 (see the upper right panel of Fig. 7). We find the same behavior of the branching ratios for the lifetimes of the $3d4d\ ^3F_2$, $3d4d\ ^1D_2$, and $3d4d\ ^1F_3$ levels presented on the center left and two bottom panels of Fig. 7.

An abrupt change of the dominant transition for very high-Z ions with $Z = 88$–92 occurs for the $3d4d\ ^3D_1$, $3d4d\ ^3P_1$, $3d4d\ ^3F_2$, $3d4d\ ^3F_3$, and $3d4d\ ^1D_2$ levels, as illustrated by the center left and bottom left panels of Fig. 6 and the two center and bottom left panels of Fig. 7, respectively. Those abrupt changes in the branching ratio is caused by the dramatic change in Z-dependences of the transition rates (see Figs. 4 and 5). We already discussed previously that singularities in the transition-rate curves could be explained one of three origins: avoided level crossings, zeros in the dipole matrix elements, and zeros in transition energies. For example, the abrupt change in the branching ratio of the $3d4d\ ^3P_1$ level (see the bottom left panels of Fig. 6) with nuclear charge $Z = 93$ is caused by the avoided level crossing of the $3d4d\ ^3P_1$ and $3d4p\ ^3D_2$ levels. There are three largest mixing coefficients $C^Q(3d_{3/2}4d_{3/2}(1))$ $C^Q(3d_{3/2}4d_{5/2}(1))$, and $C^Q(3p_{3/2}4p_{1/2}(1))$ when $Q = 3d4d\ ^3P_1$ (see Graph 4 in Ref. [3]). The value of the $C^Q(3d_{3/2}4d_{3/2}(1))$ coefficient dramatically decreases for $Z \geq 93$; however, the value of the $C^Q(3p_{3/2}4p_{1/2}(1)$ coefficient becomes equal to 1.0 for $Z \geq 93$. For high-Z ions, there is only one largest mixing coefficient $C^{Q'}(3d_{3/2}4p_{1/2}(1))$ when $Q' = 3d4p\ ^3P_1$, however, there are two largest mixing coefficient $C^{Q'}(3d_{3/2}4p_{3/2}(2))$ and $C^{Q'}(3p_{3/2}4s_{1/2}(2))$ when $Q' = 3d4p\ ^3D_2$ [3]. The

values of these coefficients are inverted when $Z = 93$. Because of this change in mixing coefficients the branching ratio of the $3d4p\ ^3D_2 - 3d4d\ ^3P_1$ transition becomes dominant for $Z \geq 93$, instead of the $3d4p\ ^3P_1 - 3d4d\ ^3P_1$ transition. The similar explanation is found for the other four $3d4d\ ^3D_1$, $3d4d\ ^3F_2$, $3d4d\ ^3F_3$, and $3d4d\ ^1D_2$ levels. All those contributions are taken into account in the calculations of the lifetime data.

The general trends of the Z-dependences of the lifetimes multiplied by $(Z-21)^2$ for the $3d4d\ ^{1,3}L_J$ levels in Ni-like ions are presented in Fig. 8. It should be noted that Z was decreased by 21 to provide better presentation of the lifetime data. The Z-dependences of lifetimes are smoother than the Z-dependence of the transition rates presented in Figs. 4 and 5. A sharp change in the trends of of the lifetimes occurs in high-Z ions for the $3d4d\ ^3D_1$ and $3d4d\ ^1D_2$ levels shown on the bottom left panel of Fig. 8. We already mentioned that the branching ratios for the $3d4d\ ^3D_1$, $3d4d\ ^3P_1$, $3d4d\ ^3F_2$, $3d4d\ ^3F_3$, and $3d4d\ ^1D_2$ levels change abruptly for high-Z ions. Abrupt changes for the $3d4d\ ^3D_1$ and $3d4d\ ^1D_2$ levels happens twice, at $Z = 87$ and 91, as shown on the central right panel of Fig. 4 and the bottom left panel of Fig. 5. Transition rates of those new transitions become larger for $Z \geq 87$ that leads to decreasing of lifetimes for the $3d4d\ ^3D_1$ and $3d4d\ ^1D_2$ levels shown in Fig. 8.

IV. CONCLUSION

We have presented a systematic second-order relativistic MBPT study of the reduced matrix elements, oscillator strengths, and transition rates for the $4s - 4p$, $4p - 4d$, $4d - 4f$, $3s - 3p$, and $3p - 3d$ electric-dipole transitions in nickelike ions with the nuclear charge Z ranging from 34 to 100. Our retarded $E1$ matrix elements include correlation corrections from Coulomb and Breit interactions. Both length and velocity forms of the matrix elements were evaluated, and small differences, caused by the non-locality of the starting DF potential, were found between the two forms. Contributions from negative energy states were also included in order to improve the agreement between results calculated in lengths and velocity gauges. Second-order RMBPT transition energies were used in our evaluation of the oscillator strengths and transition rates. These calculations are compared with other calculations and with available experimental data. For $Z \geq 36$, we believe that the present theoretical data are more accurate than other theoretical or experimental data for transitions between $n = 4$ states in Ni-like ions. We hope that these results will be useful in analyzing older experiments and planning new ones.

Acknowledgments

This research was sponsored by the National Nuclear Security Administration under Cooperative agreement 52-06NA27588. Work at LLNL was performed under auspices of the DOE under contract No. W-7405-Eng-48.

[1] U. I. Safronova, W. R. Johnson, and J. R. Albritton, Phys. Rev. A **62**, 052505 (2000).
[2] S. M. Hamasha, A. S. Shlyaptseva, and U. I. Safronova, Can. J. Phys. **82**, 331 (2004).
[3] U. Safronova, A. S. Safronova, S. M. Hamasha, and P. Beiersdorfer, At. Data Nucl. Data Tabl. **92**, 47 (2006).
[4] U. Safronova, A. S. Safronova, S. M. Hamasha, and P. Beiersdorfer, J. Phys. B **39**, 4491 (2006).
[5] R. F. Smith, J. Dunn, J. Filevich, S. Moon, J. Nilsen, R. Keenan, V. N. Shlyaptsev, J. J. Rocca, J. R. Hunter, and M. C. Marconi, Phys. Rev. E **72**, 36404 (2005).
[6] R. Keenan, J. Dunn, P. K. Patel, D. F. Price, R. F. Smith, and V. N. Shlyaptsev, Phys. Rev. Lett. **94**, 103901 (2005).
[7] T. Kawachi, A. Sasaki, M. Tanaka, M. Kishimoto, N. Hasegava, K. Nagashimo, F. Koike, H. Daido, and Y. Kato, Phys. Rev. A **69**, 33805 (2004).
[8] K. A. Janulewicz, A. Lucianetti, G. Priebe, W. Sandner, and P. V. Nickles, Phys. Rev. A **68**, 51802R (2003).
[9] T. Mocek, S. Sebban, L. M. Upcraft, I. Bettaibi, P. B. G. Grillon, B. Rus, D. Ros, A. Klisnick, A. Carillon, G. Jamelot, et al., Proceedings of SPIE **5197**, 119 (2003).
[10] P. A. Norreys, J. Zhang, G. Cairns, A. Djaoui, L. Dwivedi, M. H. Key, R. Kodama, J. Krishnan, C. L. S. Lewis, D. Neely, et al., J. Phys. B **26**, 3693 (1993).
[11] J. H. Scofield and B. J. MacGowa, Phys. Scr. **46**, 361 (1992).
[12] M. H. Chen and A. L. Osterheld, Phys. Rev. A **52**, 3790 (1995).
[13] Y. Li, J. Nilsen, J. Dunn, A. L. Osterheld, A. Ryabtsev, and S. Churilov, Phys. Rev. A **58**, R2668 (1998).
[14] H. Daido, S. Ninomiya, M. Takagi, Y. Kato, and F. Koike, J. Opt. Soc. Am. B **16**, 296 (1999).
[15] J. Nilsen, J. Dunn, A. L. Osterheld, and Y. Li, Phys. Rev. A **60**, R2677 (1999).
[16] R. King, G. J. P. K. M. Aggarwal, F. P. Keenman, and S. J. Rose, J. Phys. B **37**, 225 (2004).
[17] P. Beiersdorfer, J. Nilsen, A. Osterheld, D. Vogel, K. Wong, R. Marrs, and R. Zasadzinski, Phys. Rev. A **46**, R25 (1992).
[18] S. R. Elliott, P. Beiersdorfer, B. J. MacGowan, and J. Nilsen, Phys. Rev. A **51**, 1683 (1995).

TABLE I: Contributions to E1 uncoupled reduced matrix elements (a.u.) in length L and velocity V forms for transitions between excited states $av(J)$ and $a'v'(J')$ in W^{46+}.

Coulomb interaction						
$av(J)$	$a'v'(J')$		$Z^{(\mathrm{DF})}$	$P^{(\mathrm{derv})}$	$Z^{(\mathrm{RPA})}$	$Z^{(\mathrm{corr})}$
$3p_{1/2}4s_{1/2}(1)$	$3s_{1/2}4s_{1/2}(0)$	(L)	0.109213	0.109226	-0.010600	-0.000003
		(V)	0.104743	0.000032	-0.005844	-0.003954
$3s_{1/2}4p_{1/2}(1)$	$3s_{1/2}4s_{1/2}(0)$	(L)	-0.224466	-0.224476	0.007251	0.002028
		(V)	-0.226091	-0.000027	0.008468	0.011603
$3d_{5/2}4p_{3/2}(1)$	$3p_{3/2}4p_{3/2}(1)$	(L)	-0.128829	-0.128748	0.011751	-0.001239
		(V)	-0.123294	0.000140	0.005980	-0.001724
$3d_{3/2}4p_{3/2}(1)$	$3d_{3/2}4d_{5/2}(1)$	(L)	0.291004	0.290928	-0.008509	-0.003593
		(V)	0.294810	-0.000125	-0.011747	0.002303
$3p_{1/2}4s_{1/2}(1)$	$3s_{1/2}4s_{1/2}(1)$	(L)	-0.154450	-0.154470	0.014990	-0.000954
		(V)	-0.148130	-0.000046	0.008264	-0.001643
$3p_{3/2}4d_{3/2}(1)$	$3d_{5/2}4d_{3/2}(1)$	(L)	-0.128829	-0.128748	0.011751	0.000317
		(V)	-0.123294	0.000140	0.005980	0.004688
$3p_{3/2}4d_{5/2}(1)$	$3d_{5/2}4d_{5/2}(1)$	(L)	-0.160678	-0.160577	0.014656	0.000472
		(V)	-0.153774	0.000174	0.007458	0.002461
$3s_{1/2}4p_{3/2}(1)$	$3p_{1/2}4p_{3/2}(1)$	(L)	0.077225	0.077235	-0.007495	-0.000527
		(V)	0.074065	0.000023	-0.004132	-0.000029
$3p_{3/2}4d_{3/2}(1)$	$3d_{5/2}4d_{3/2}(2)$	(L)	0.196790	0.196666	-0.017950	-0.000011
		(V)	0.188335	-0.000214	-0.009135	-0.000785
$3p_{3/2}4d_{5/2}(1)$	$3d_{5/2}4d_{5/2}(2)$	(L)	0.131193	0.131111	-0.011967	-0.000670
		(V)	0.125556	-0.000142	-0.006090	-0.003306
$3p_{3/2}4d_{5/2}(1)$	$3p_{3/2}4p_{3/2}(2)$	(L)	-0.097001	-0.096976	0.002836	0.001062
		(V)	-0.098270	0.000042	0.003916	-0.001250
$3s_{1/2}4p_{3/2}(1)$	$3p_{1/2}4p_{3/2}(2)$	(L)	-0.172681	-0.172702	0.016759	-0.001399
		(V)	-0.165614	-0.000051	0.009239	-0.002606
Coulomb-Breit interaction						
$av(J)$	$a'v'(J')$		$B^{(\mathrm{HF})}$	$B^{(\mathrm{RPA})}$	$B^{(\mathrm{corr})}$	$B^{(2)}$
$3p_{1/2}4s_{1/2}(1)$	$3s_{1/2}4s_{1/2}(0)$	(L)	0.000187	-0.000015	0.000002	0.000174
		(V)	0.001605	-0.000093	-0.000006	0.001506
$3s_{1/2}4p_{1/2}(1)$	$3s_{1/2}4s_{1/2}(0)$	(L)	-0.000289	0.000010	0.000008	-0.000272
		(V)	-0.002579	-0.000117	0.000340	-0.002356
$3d_{5/2}4p_{3/2}(1)$	$3p_{3/2}4p_{3/2}(1)$	(L)	-0.000136	0.000020	-0.000014	-0.000130
		(V)	0.000745	0.000149	-0.000004	0.000890
$3d_{3/2}4p_{3/2}(1)$	$3d_{3/2}4d_{5/2}(1)$	(L)	0.000228	-0.000006	0.000034	0.000257
		(V)	-0.001470	0.000145	0.000281	-0.001045
$3p_{1/2}4s_{1/2}(1)$	$3s_{1/2}4s_{1/2}(1)$	(L)	-0.000265	0.000022	0.000000	-0.000243
		(V)	-0.002270	0.000131	0.000085	-0.002054
$3p_{3/2}4d_{3/2}(1)$	$3d_{5/2}4d_{3/2}(1)$	(L)	-0.000136	0.000020	0.000006	-0.000110
		(V)	0.000745	0.000149	0.000044	0.000939
$3p_{3/2}4d_{5/2}(1)$	$3d_{5/2}4d_{5/2}(1)$	(L)	-0.000170	0.000025	-0.000123	-0.000267
		(V)	0.000929	0.000186	-0.000221	0.000894
$3s_{1/2}4p_{3/2}(1)$	$3p_{1/2}4p_{3/2}(1)$	(L)	0.000133	-0.000011	0.000004	0.000125
		(V)	0.001135	-0.000066	-0.000019	0.001050
$3p_{3/2}4d_{3/2}(1)$	$3d_{5/2}4d_{3/2}(2)$	(L)	0.000208	-0.000031	0.000005	0.000182
		(V)	-0.001138	-0.000228	-0.000028	-0.001394
$3p_{3/2}4d_{5/2}(1)$	$3d_{5/2}4d_{5/2}(2)$	(L)	0.000139	-0.000021	0.000016	0.000134
		(V)	-0.000759	-0.000152	-0.000071	-0.000981
$3p_{3/2}4d_{5/2}(1)$	$3p_{3/2}4p_{3/2}(2)$	(L)	-0.000076	0.000002	0.000015	-0.000059
		(V)	0.000490	-0.000048	0.000056	0.000498
$3s_{1/2}4p_{3/2}(1)$	$3p_{1/2}4p_{3/2}(2)$	(L)	-0.000296	0.000024	-0.000018	-0.000290
		(V)	-0.002538	0.000147	-0.000108	-0.002499

TABLE II: Coupled reduced matrix elements Q calculated in length L and velocity V forms for W^{46+}.

		First order		RMBPT			
$l_1 l_2$ LSJ	$l_3 l_4$ $L'S'J'$	L	V	L	V	$j_1 j_2$ (J)	$j_3 j_4$ (J')
$3p4s\ ^3P_1$	$3s4s\ ^1S_0$	0.10599	0.10159	0.09605	0.09607	$3p_{1/2}4s_{1/2}(1)$	$3s_{1/2}4s_{1/2}(0)$
$3s4p\ ^3P_1$	$3s4s\ ^1S_0$	0.10749	0.10830	0.10230	0.10229	$3s_{1/2}4p_{1/2}(1)$	$3s_{1/2}4s_{1/2}(0)$
$3d4p\ ^3D_1$	$3p4p\ ^3S_1$	0.12901	0.12370	0.11866	0.11859	$3d_{5/2}4p_{3/2}(1)$	$3p_{3/2}4p_{3/2}(1)$
$3d4p\ ^1P_1$	$3d4d\ ^3P_1$	0.28177	0.28558	0.27197	0.27192	$3d_{3/2}4p_{3/2}(1)$	$3d_{3/2}4d_{5/2}(1)$
$3d4f\ ^3D_1$	$3d4d\ ^3S_1$	0.30533	0.31464	0.29029	0.29027	$3d_{5/2}4f_{7/2}(1)$	$3d_{5/2}4d_{3/2}(1)$
$3p4s\ ^3P_1$	$3s4s\ ^3S_1$	0.20389	0.19756	0.18871	0.18867	$3p_{1/2}4s_{1/2}(1)$	$3s_{1/2}4s_{1/2}(1)$
$3p4d\ ^3P_1$	$3d4d\ ^3S_1$	0.11225	0.10696	0.10064	0.10058	$3p_{3/2}4d_{3/2}(1)$	$3d_{5/2}4d_{3/2}(1)$
$3p4d\ ^1P_1$	$3d4d\ ^1P_1$	0.15140	0.14468	0.13787	0.13775	$3p_{3/2}4d_{5/2}(1)$	$3d_{5/2}4d_{5/2}(1)$
$3s4p\ ^1P_1$	$3p4p\ ^3P_1$	0.13236	0.12887	0.12200	0.12206	$3s_{1/2}4p_{3/2}(1)$	$3p_{1/2}4p_{3/2}(1)$
$3d4f\ ^3P_1$	$3d4s\ ^1D_2$	0.03299	0.03136	0.02999	0.03000	$3d_{5/2}4f_{5/2}(1)$	$3d_{3/2}4s_{1/2}(2)$
$3d4f\ ^1P_1$	$3p4f\ ^3D_2$	0.06562	0.06243	0.05445	0.05442	$3d_{3/2}4f_{5/2}(1)$	$3p_{3/2}4f_{5/2}(2)$
$3p4s\ ^3P_1$	$3s4d\ ^1D_2$	0.01202	0.01147	0.01209	0.01209	$3p_{1/2}4s_{1/2}(1)$	$3s_{1/2}4d_{5/2}(2)$
$3p4d\ ^3P_1$	$3d4d\ ^3P_2$	0.19227	0.18404	0.17436	0.17426	$3p_{3/2}4d_{3/2}(1)$	$3d_{5/2}4d_{3/2}(2)$
$3p4d\ ^3P_1$	$3d4d\ ^1D_2$	0.05844	0.05574	0.05324	0.05321	$3p_{3/2}4d_{3/2}(1)$	$3d_{3/2}4d_{3/2}(2)$
$3p4d\ ^1P_1$	$3d4d\ ^3P_2$	0.01293	0.01231	0.01220	0.01220	$3p_{3/2}4d_{5/2}(1)$	$3d_{5/2}4d_{3/2}(2)$
$3p4d\ ^1P_1$	$3d4d\ ^3D_2$	0.12787	0.12231	0.11579	0.11577	$3p_{3/2}4d_{5/2}(1)$	$3d_{5/2}4d_{5/2}(2)$
$3p4d\ ^1P_1$	$3d4d\ ^1D_2$	0.07050	0.06718	0.06456	0.06457	$3p_{3/2}4d_{5/2}(1)$	$3d_{3/2}4d_{5/2}(2)$
$3p4d\ ^1P_1$	$3p4p\ ^1D_2$	0.07634	0.07750	0.07356	0.07360	$3p_{3/2}4d_{5/2}(1)$	$3p_{3/2}4p_{3/2}(2)$
$3s4p\ ^3P_1$	$3s4d\ ^1D_2$	0.01113	0.01092	0.01022	0.01022	$3s_{1/2}4p_{1/2}(1)$	$3s_{1/2}4d_{5/2}(2)$
$3s4p\ ^1P_1$	$3p4p\ ^3P_2$	0.17015	0.16304	0.15615	0.15606	$3s_{1/2}4p_{3/2}(1)$	$3p_{1/2}4p_{3/2}(2)$

TABLE III: Level inversions in Ni-like ions.

			3d4d				3d4d				3d4d	
Levels	$^3P_1$	$^3D_1$	$^1P_1$	$^3S_1$	$^1D_2$	$^3F_2$	$^3D_2$	$^3P_2$	$^1F_3$	$^3F_3$	$^3D_3$	$^3F_4$	$^3G_4$
$3d4f\ ^3P_2$	77	80	89		76	79	88		76	80	88		
$3d4f\ ^3D_2$									95				
$3d4f\ ^1D_2$									99				
$3d4f\ ^3D_3$									96			97	
$3d4f\ ^3G_3$									100				
$3d4f\ ^3H_4$									96			97	
$3d4f\ ^3G_4$									99				
$3d4f\ ^3H_5$												96	
$3d4f\ ^3G_5$												100	
$3d4p\ ^3P_0$				95									
$3d4p\ ^3D_2$				94									
$3d4p\ ^3D_3$								95					95

[19] S. R. Elliott, P. Beiersdorfer, B. J. MacGowan, and J. Nilsen, Phys. Rev. A **52**, 2689 (1995).
[20] M. J. May, K. B. Fournier, P. Beiersdorfer, H. Chen, and K. L. Wong, Phys. Rev. E **68**, 36402 (2003).
[21] A. Shlyaptseva, D. Fedin, S.Hamasha, C. Harris, V. Kantsyrev, P. Neill, N. Quart, U. I. Safronova, P. Beiersdorfer, K. Boyce, et al., Rev. Scientific Instr. B **75**, 3750 (2004).
[22] P. Neill, C. Harris, A. S. Safronova, S. M. Hamasha, S. Hansen, U. Safronova, and P. Beiersdorfer, Can. J. Phys. **82**, 931 (2004).
[23] R. Doron, M. Fraenkel, P. Mandelbaum, A. Zigler, and J. J. Schwob, Phys. Scr. **58**, 19 (1998).
[24] A. Zigler, P. Mandelbaum, J. J. Schwob, and D. Mitnik, Phys. Scr. **50**, 61 (1994).
[25] R. Doron, E. B. M. Fraenkel, P. Mandelbaum, , J. J. Schwob, A. Zigler, A. Y. Faenov, and T. A. Pikuz, Phys. Rev. A **62**, 52508 (2000).
[26] S. von Goeler, P. Beiersdorfer, M. Bitter, R. Bell, K. Hill, P. LaSalle, L. Ratzan, J. Stevens, J. Timberlake, S. Maxon, et al., J. Phys. (Paris) Colloq. C1 **49**, 349 (1988).
[27] R. Neu, K. B. Fournier, D. Schlgl, and J. Rice, J. Phys. B **30**, 5057 (1997).
[28] K. B. Fournier, At. Data Nucl. Data Tabl. **68**, 1 (1998).
[29] M. Klapisch, J. J. Schwob, M. Fraenkel, and J. Oreg, J. Opt. Soc. Am. **61**, 148 (1977).
[30] H. L. Zhang, D. H. Sampson, and C. J. Fonts, At. Data Nucl. Data Tabl. **48**, 91 (1991).
[31] S. Elliott, P. Beiersdorfer, and J. Nilsen, Phys. Scr. **49**, 556 (1994).

TABLE IV: Wavelengths (λ in $\AA$) and transition rates (gA in $10^9 s^{-1}$) for $3d4p - 3d4d$ transitions in Ni-like krypton, Z=36. The RMBPT results are compared with experimental measurements by Churilov *et al.* in Ref. [42].

Tran., jj-coupl.		λ in $\AA$		gA in $10^9 s^{-1}$		Tran., LS-coupl.	
Lower	Upper	RMBPT	expt	RMBPT	expt	Lower	Upper
$3d_{5/2}4p_{3/2}$ (1)	$3d_{3/2}4d_{3/2}$ (0)	345.000	328.640	29.1	34.9	$3d4p\ ^1P_1$	$3d4d\ ^1S_0$
$3d_{3/2}4p_{1/2}$ (1)	$3d_{5/2}4d_{5/2}$ (0)	401.367	401.993	22.8	23.8	$3d4p\ ^3P_1$	$3d4d\ ^3P_0$
$3d_{3/2}4p_{3/2}$ (1)	$3d_{5/2}4d_{5/2}$ (0)	437.084	437.935	0.9	0.9	$3d4p\ ^3D_1$	$3d4d\ ^3P_0$
$3d_{3/2}4p_{1/2}$ (1)	$3d_{3/2}4d_{3/2}$ (1)	399.558	398.826	15.6	14.2	$3d4p\ ^3P_1$	$3d4d\ ^3P_1$
$3d_{3/2}4p_{3/2}$ (0)	$3d_{3/2}4d_{3/2}$ (1)	411.080	409.612	11.5	11.1	$3d4p\ ^3P_0$	$3d4d\ ^3P_1$
$3d_{5/2}4p_{3/2}$ (1)	$3d_{3/2}4d_{3/2}$ (1)	423.113	423.260	11.0	10.6	$3d4p\ ^1P_1$	$3d4d\ ^3P_1$
$3d_{3/2}4p_{3/2}$ (1)	$3d_{3/2}4d_{3/2}$ (1)	434.939	434.170	12.8	14.1	$3d4p\ ^3D_1$	$3d4d\ ^3P_1$
$3d_{3/2}4p_{3/2}$ (2)	$3d_{3/2}4d_{3/2}$ (1)	438.181	437.838	11.8	11.0	$3d4p\ ^3D_2$	$3d4d\ ^3P_1$
$3d_{3/2}4p_{1/2}$ (1)	$3d_{3/2}4d_{5/2}$ (1)	393.254	392.537	6.0	8.3	$3d4p\ ^3P_1$	$3d4d\ ^3D_1$
$3d_{5/2}4p_{3/2}$ (2)	$3d_{3/2}4d_{5/2}$ (1)	396.486	396.295	6.4	5.6	$3d4p\ ^3F_2$	$3d4d\ ^3D_1$
$3d_{3/2}4p_{3/2}$ (0)	$3d_{3/2}4d_{5/2}$ (1)	404.411	402.961	24.5	25.7	$3d4p\ ^3P_0$	$3d4d\ ^3D_1$
$3d_{5/2}4p_{3/2}$ (1)	$3d_{3/2}4d_{5/2}$ (1)	416.050	416.159	17.3	19.6	$3d4p\ ^1P_1$	$3d4d\ ^3D_1$
$3d_{3/2}4p_{3/2}$ (1)	$3d_{3/2}4d_{5/2}$ (1)	427.480	426.708	13.9	11.0	$3d4p\ ^3D_1$	$3d4d\ ^3D_1$
$3d_{5/2}4p_{1/2}$ (2)	$3d_{5/2}4d_{3/2}$ (1)	408.261	413.728	47.9	50.3	$3d4p\ ^3P_2$	$3d4d\ ^3S_1$
$3d_{3/2}4p_{1/2}$ (1)	$3d_{5/2}4d_{3/2}$ (1)	427.610	433.066	10.5	12.0	$3d4p\ ^3P_1$	$3d4d\ ^3S_1$
$3d_{5/2}4p_{1/2}$ (2)	$3d_{5/2}4d_{5/2}$ (1)	393.451	393.244	12.8	16.1	$3d4p\ ^3P_2$	$3d4d\ ^1P_1$
$3d_{3/2}4p_{1/2}$ (1)	$3d_{5/2}4d_{5/2}$ (1)	411.391	410.676	17.3	18.5	$3d4p\ ^3P_1$	$3d4d\ ^1P_1$
$3d_{3/2}4p_{1/2}$ (2)	$3d_{5/2}4d_{5/2}$ (1)	430.632	429.881	9.7	10.3	$3d4p\ ^1D_2$	$3d4d\ ^1P_1$
$3d_{5/2}4p_{3/2}$ (1)	$3d_{5/2}4d_{5/2}$ (1)	436.406	436.640	14.1	14.7	$3d4p\ ^1P_1$	$3d4d\ ^1P_1$
$3d_{5/2}4p_{3/2}$ (2)	$3d_{3/2}4d_{3/2}$ (2)	390.845	389.737	6.2	8.7	$3d4p\ ^3F_2$	$3d4d\ ^3F_2$
$3d_{3/2}4p_{3/2}$ (1)	$3d_{3/2}4d_{3/2}$ (2)	420.930	419.130	58.3	66.1	$3d4p\ ^3D_1$	$3d4d\ ^3F_2$
$3d_{3/2}4p_{3/2}$ (2)	$3d_{3/2}4d_{3/2}$ (2)	423.966	422.533	33.2	29.3	$3d4p\ ^3D_2$	$3d4d\ ^3F_2$
$3d_{5/2}4p_{3/2}$ (2)	$3d_{3/2}4d_{5/2}$ (2)	387.285	386.632	32.4	33.3	$3d4p\ ^3F_2$	$3d4d\ ^1D_2$
$3d_{3/2}4p_{1/2}$ (2)	$3d_{3/2}4d_{5/2}$ (2)	400.931	399.709	10.9	11.7	$3d4p\ ^1D_2$	$3d4d\ ^1D_2$
$3d_{5/2}4p_{3/2}$ (1)	$3d_{3/2}4d_{5/2}$ (2)	405.931	405.530	37.4	45.0	$3d4p\ ^1P_1$	$3d4d\ ^1D_2$
$3d_{3/2}4p_{3/2}$ (1)	$3d_{3/2}4d_{5/2}$ (2)	416.804	415.530	9.4	6.9	$3d4p\ ^3D_1$	$3d4d\ ^1D_2$
$3d_{3/2}4p_{3/2}$ (2)	$3d_{3/2}4d_{5/2}$ (2)	419.780	418.899	16.6	19.9	$3d4p\ ^3D_2$	$3d4d\ ^1D_2$
$3d_{5/2}4p_{1/2}$ (2)	$3d_{5/2}4d_{3/2}$ (2)	390.896	393.075	78.6	86.9	$3d4p\ ^3P_2$	$3d4d\ ^3P_2$
$3d_{5/2}4p_{1/2}$ (3)	$3d_{5/2}4d_{3/2}$ (2)	400.252	401.899	8.2	9.3	$3d4p\ ^3F_3$	$3d4d\ ^3F_2$
$3d_{5/2}4p_{3/2}$ (3)	$3d_{5/2}4d_{3/2}$ (2)	430.089	432.351	20.4	21.5	$3d4p\ ^3D_3$	$3d4d\ ^3P_2$
$3d_{3/2}4p_{1/2}$ (1)	$3d_{5/2}4d_{5/2}$ (2)	401.380	400.529	31.3	36.1	$3d4p\ ^3P_1$	$3d4d\ ^3D_2$
$3d_{5/2}4p_{3/2}$ (2)	$3d_{5/2}4d_{5/2}$ (2)	404.749		11.4		$3d4p\ ^3F_2$	$3d4d\ ^3D_2$
$3d_{3/2}4p_{1/2}$ (2)	$3d_{5/2}4d_{5/2}$ (2)	419.676	418.783	44.1	48.1	$3d4p\ ^1D_2$	$3d4d\ ^3D_2$
$3d_{3/2}4p_{3/2}$ (2)	$3d_{5/2}4d_{5/2}$ (2)	440.374	439.900	4.6	6.2	$3d4p\ ^3D_2$	$3d4d\ ^3D_2$
$3d_{5/2}4p_{1/2}$ (3)	$3d_{3/2}4d_{3/2}$ (3)	386.978	385.676	8.0	18.2	$3d4p\ ^3F_3$	$3d4d\ ^1F_3$
$3d_{5/2}4p_{3/2}$ (2)	$3d_{3/2}4d_{3/2}$ (3)	398.033	397.394	64.4	56.0	$3d4p\ ^3F_2$	$3d4d\ ^1F_3$
$3d_{3/2}4p_{1/2}$ (2)	$3d_{3/2}4d_{3/2}$ (3)	412.460	411.217	61.4	86.5	$3d4p\ ^1D_2$	$3d4d\ ^1F_3$
$3d_{3/2}4p_{3/2}$ (3)	$3d_{3/2}4d_{3/2}$ (3)	422.300	423.915	7.2	8.7	$3d4p\ ^3D_3$	$3d4d\ ^3G_3$
$3d_{3/2}4p_{3/2}$ (2)	$3d_{3/2}4d_{3/2}$ (3)	432.436	431.547	3.3	3.3	$3d4p\ ^1D_2$	$3d4d\ ^1F_3$
$3d_{3/2}4p_{3/2}$ (3)	$3d_{3/2}4d_{5/2}$ (3)	410.566	409.432	35.4	33.3	$3d4p\ ^3F_3$	$3d4d\ ^1F_3$
$3d_{3/2}4p_{3/2}$ (2)	$3d_{3/2}4d_{5/2}$ (3)	420.140	418.926	101.2	114.1	$3d4p\ ^3D_2$	$3d4d\ ^3F_3$
$3d_{5/2}4p_{1/2}$ (2)	$3d_{5/2}4d_{3/2}$ (3)	388.512	388.717	47.4	52.9	$3d4p\ ^3P_2$	$3d4d\ ^3D_3$
$3d_{5/2}4p_{1/2}$ (3)	$3d_{5/2}4d_{3/2}$ (3)	397.752	397.329	25.2	28.2	$3d4p\ ^3F_3$	$3d4d\ ^3D_3$
$3d_{5/2}4p_{3/2}$ (4)	$3d_{5/2}4d_{3/2}$ (3)	411.061		11.8		$3d4p\ ^3F_4$	$3d4d\ ^3D_3$
$3d_{5/2}4p_{3/2}$ (3)	$3d_{5/2}4d_{3/2}$ (3)	427.204	427.064	54.5	56.8	$3d4p\ ^3D_3$	$3d4d\ ^3D_3$
$3d_{3/2}4p_{3/2}$ (3)	$3d_{5/2}4d_{3/2}$ (3)	435.163	435.437	10.3	13.9	$3d4p\ ^1F_3$	$3d4d\ ^3D_3$
$3d_{5/2}4p_{1/2}$ (3)	$3d_{5/2}4d_{5/2}$ (3)	395.445	394.596	35.0	31.0	$3d4p\ ^3F_3$	$3d4d\ ^3G_3$
$3d_{5/2}4p_{3/2}$ (2)	$3d_{5/2}4d_{5/2}$ (3)	406.997	406.864	62.0	94.8	$3d4p\ ^3F_2$	$3d4d\ ^3G_3$
$3d_{3/2}4p_{1/2}$ (2)	$3d_{5/2}4d_{5/2}$ (3)	422.094	421.368	40.2	28.8	$3d4p\ ^1D_2$	$3d4d\ ^3G_3$
$3d_{3/2}4p_{3/2}$ (2)	$3d_{5/2}4d_{5/2}$ (3)	443.037	442.752	0.8	1.6	$3d4p\ ^1D_2$	$3d4d\ ^3G_3$
$3d_{3/2}4p_{3/2}$ (3)	$3d_{3/2}4d_{5/2}$ (4)	418.412	417.594	168.3	194.5	$3d4p\ ^1F_3$	$3d4d\ ^1G_4$
$3d_{5/2}4p_{1/2}$ (3)	$3d_{5/2}4d_{3/2}$ (4)	403.991	403.214	177.8	205.3	$3d4p\ ^3F_3$	$3d4d\ ^3G_4$
$3d_{5/2}4p_{3/2}$ (4)	$3d_{5/2}4d_{3/2}$ (4)	417.728		12.3		$3d4p\ ^3F_4$	$3d4d\ ^3G_4$
$3d_{5/2}4p_{3/2}$ (3)	$3d_{5/2}4d_{3/2}$ (4)	434.409	433.885	6.4	7.1	$3d4p\ ^3D_3$	$3d4d\ ^3G_4$
$3d_{5/2}4p_{3/2}$ (4)	$3d_{5/2}4d_{5/2}$ (4)	405.163	404.403	55.7	54.6	$3d4p\ ^3F_4$	$3d4d\ ^3F_4$
$3d_{5/2}4p_{3/2}$ (3)	$3d_{5/2}4d_{5/2}$ (4)	420.837	420.398	131.5	153.1	$3d4p\ ^3D_3$	$3d4d\ ^3F_4$
$3d_{5/2}4p_{3/2}$ (4)	$3d_{5/2}4d_{5/2}$ (5)	417.814	416.756	224.2	255.1	$3d4p\ ^3F_4$	$3d4d\ ^3G_5$

TABLE V: Wavelengths (λ in $\AA$) and transition rates (gA in $10^9 s^{-1}$) for $3d4s-3d4p$ transitions in Ni-like Pd^{18+}. The RMBPT results are compared with experimental measurements by Churilov *et al.* in Ref. [36].

Transitions		RMBPT	Expt.	RMBPT	Expt.
$3d4s$	$3d4p$	λ in $\AA$	λ in $\AA$	gA	Int.
$^3D_3$	$^3D_3$	264.927	264.832	13,4	12
$^3D_1$	$^3D_2$	265.997	266.435	8.41	5
$^3D_2$	$^3D_3$	268.927	269.247	7.23	9
$^3D_1$	$^3D_1$	269.941	271.523	1.73	8
$^1D_2$	$^3D_2$	270.298	270.183	1.20	9
$^3D_2$	$^1P_1$	271.542	271.523	10.7	8
$^3D_2$	$^3F_2$	274.197	274.645	16.0	17
$^3D_3$	$^3F_4$	277.674	277.985	18.3	20
$^1D_2$	$^1F_3$	277.727	277.610	18.0	17
$^3D_1$	$^3P_0$	284.250	287.837	18.1	3
$^3D_2$	$^3P_1$	289.793	289.330	6.93	3
$^3D_2$	$^1D_2$	293.548	293.810	1.82	3
$^3D_1$	$^1P_1$	303.626	303.895	2.07	3
$^1D_2$	$^1P_1$	309.244	308.776	4.50	3
$^3D_3$	$^3F_3$	326.636	326.804	4.09	8
$^3D_1$	$^1D_2$	331.406	332.095	5.67	10
$^3D_2$	$^3F_3$	332.738	333.550	6.57	8
$^1D_2$	$^3P_1$	333.137	332.010	6.37	5
$^3D_3$	$^3P_2$	335.292	334.356	9.96	15
$^1D_2$	$^1D_2$	338.109	337.928	3.44	10

TABLE VI: Wavelengths (λ in $\AA$) and transition rates (gA in $10^{10} s^{-1}$) for $3d4p-3d4d$ transitions in Ni-like ions. The RMBPT results are compared with experimental measurements by MacGowan *et al.* in Ref. [37] (Z=63 and 70), Ref. [38] (Z=73 and 74), and Ref. [39] (Z=79).

Ion	Expt.	RMBPT	RMBPT
	λ in $\AA$	λ in $\AA$	gA
	$3d_{5/2}4p_{3/2}$ (1) $-$ $3d_{5/2}4d_{5/2}$ (1)		
$Z=79$		65.54	24.0
$Z=74$	75.35 $\pm$0.015	75.30	19.1
$Z=73$	77.47 $\pm$0.02	77.47	18.2
$Z=70$	84.40 $\pm$0.05	84.47	15.8
$Z=63$	104.56$\pm$0.05	104.57	11.2
	$3d_{5/2}4p_{3/2}$ (1) $-$ $3d_{5/2}4d_{5/2}$ (2)		
$Z=79$		63.02	11.5
$Z=74$	72.40 $\pm$0.015	72.33	9.21
$Z=73$	74.42 $\pm$0.02	74.40	8.81
$Z=70$		81.09	7.70
$Z=63$	100.39$\pm$0.05	100.37	5.55
	$3d_{5/2}4p_{3/2}$ (1) $-$ $3d_{3/2}4d_{3/2}$ (0)		
$Z=79$		42.24	41.2
$Z=74$		49.46	37.7
$Z=73$	50.97$\pm$0.02	51.07	37.0
$Z=70$	56.09$\pm$0.05	56.26	34.8
$Z=63$	71.00$\pm$0.03	71.10	29.4
	$3d_{3/2}4p_{1/2}$ (1) $-$ $3d_{3/2}4d_{3/2}$ (0)		
$Z=79$	35.605$\pm$0.02	35.71	132.
$Z=74$	43.185$\pm$0.01	43.231	81.9
$Z=73$	44.83 $\pm$0.02	44.91	74.1
$Z=70$	50.26 $\pm$0.05	50.35	55.0
$Z=63$	65.83 $\pm$0.03	65.98	26.8

TABLE VII: Lifetime values (τ in 10^{-9}s) of levels of Ni-like ions.

Level	Z=36	Z=37	Z=38	Z=39	Z=40	Z=41	Z=42	Z=44	Z=46	Z=47	Z=48	Z=50	Level-jj
$3d4d\ ^1S_0$	2.72[-2]	2.03[-2]	1.64[-2]	1.37[-2]	1.16[-2]	1.01[-2]	8.75[-3]	6.80[-3]	5.67[-3]	5.16[-3]	4.66[-3]	3.96[-3]	$3d_{3/2}4d_{3/2}(0)$
$3d4d\ ^3P_0$	4.11[-2]	3.70[-2]	3.14[-2]	2.72[-2]	2.39[-2]	2.11[-2]	1.90[-2]	1.54[-2]	1.30[-2]	1.19[-2]	1.10[-2]	9.55[-3]	$3d_{5/2}4d_{5/2}(0)$
$3d4d\ ^1P_1$	4.95[-2]	4.14[-2]	3.52[-2]	3.08[-2]	2.71[-2]	2.42[-2]	2.18[-2]	1.79[-2]	1.55[-2]	1.43[-2]	1.33[-2]	1.17[-2]	$3d_{5/2}4d_{5/2}(1)$
$3d4d\ ^3S_1$	4.75[-2]	4.07[-2]	3.49[-2]	3.04[-2]	2.69[-2]	2.38[-2]	2.13[-2]	1.74[-2]	1.46[-2]	1.33[-2]	1.21[-2]	1.03[-2]	$3d_{5/2}4d_{3/2}(1)$
$3d4d\ ^3P_1$	4.36[-2]	4.05[-2]	3.45[-2]	2.99[-2]	2.63[-2]	2.33[-2]	2.09[-2]	1.69[-2]	1.41[-2]	1.27[-2]	1.18[-2]	9.83[-3]	$3d_{3/2}4d_{3/2}(1)$
$3d4d\ ^3D_1$	4.28[-2]	3.90[-2]	3.31[-2]	2.86[-2]	2.53[-2]	2.24[-2]	2.02[-2]	1.66[-2]	1.43[-2]	1.31[-2]	1.22[-2]	1.08[-2]	$3d_{3/2}4d_{5/2}(1)$
$3d4d\ ^1D_2$	4.28[-2]	3.63[-2]	3.06[-2]	2.64[-2]	2.30[-2]	2.02[-2]	1.80[-2]	1.45[-2]	1.49[-2]	1.38[-2]	1.28[-2]	1.12[-2]	$3d_{3/2}4d_{5/2}(2)$
$3d4d\ ^3P_2$	4.39[-2]	3.66[-2]	3.12[-2]	2.69[-2]	2.36[-2]	2.09[-2]	1.86[-2]	1.51[-2]	1.25[-2]	1.13[-2]	1.04[-2]	8.81[-3]	$3d_{5/2}4d_{3/2}(2)$
$3d4d\ ^3D_2$	4.60[-2]	3.86[-2]	3.28[-2]	2.87[-2]	2.52[-2]	2.25[-2]	2.02[-2]	1.66[-2]	1.42[-2]	1.31[-2]	1.23[-2]	1.07[-2]	$3d_{5/2}4d_{5/2}(2)$
$3d4d\ ^3F_2$	4.52[-2]	3.98[-2]	3.40[-2]	2.97[-2]	2.61[-2]	2.33[-2]	2.10[-2]	1.73[-2]	1.19[-2]	1.09[-2]	9.95[-3]	8.36[-3]	$3d_{3/2}4d_{3/2}(2)$
$3d4d\ ^1F_3$	4.62[-2]	3.81[-2]	3.24[-2]	2.79[-2]	2.44[-2]	2.14[-2]	1.90[-2]	1.53[-2]	1.25[-2]	1.13[-2]	1.04[-2]	8.68[-3]	$3d_{5/2}4d_{3/2}(3)$
$3d4d\ ^3D_3$	4.74[-2]	3.78[-2]	3.20[-2]	2.76[-2]	2.41[-2]	2.13[-2]	1.90[-2]	1.52[-2]	1.26[-2]	1.15[-2]	1.05[-2]	8.86[-3]	$3d_{3/2}4d_{3/2}(3)$
$3d4d\ ^3F_3$	4.71[-2]	3.97[-2]	3.40[-2]	2.95[-2]	2.61[-2]	2.32[-2]	2.09[-2]	1.74[-2]	1.47[-2]	1.37[-2]	1.27[-2]	1.11[-2]	$3d_{3/2}4d_{5/2}(3)$
$3d4d\ ^3G_3$	4.68[-2]	3.90[-2]	3.32[-2]	2.90[-2]	2.56[-2]	2.29[-2]	2.06[-2]	1.71[-2]	1.47[-2]	1.36[-2]	1.27[-2]	1.12[-2]	$3d_{5/2}4d_{5/2}(3)$
$3d4d\ ^1G_4$	5.11[-2]	4.09[-2]	3.51[-2]	3.06[-2]	2.71[-2]	2.42[-2]	2.18[-2]	1.82[-2]	1.54[-2]	1.43[-2]	1.34[-2]	1.17[-2]	$3d_{3/2}4d_{5/2}(4)$
$3d4d\ ^3F_4$	4.80[-2]	4.01[-2]	3.43[-2]	2.98[-2]	2.63[-2]	2.34[-2]	2.11[-2]	1.74[-2]	1.48[-2]	1.37[-2]	1.27[-2]	1.11[-2]	$3d_{5/2}4d_{5/2}(4)$
$3d4d\ ^3G_4$	4.57[-2]	3.84[-2]	3.25[-2]	2.79[-2]	2.45[-2]	2.16[-2]	1.92[-2]	1.55[-2]	1.28[-2]	1.16[-2]	1.06[-2]	8.93[-3]	$3d_{5/2}4d_{3/2}(4)$
$3d4d\ ^3G_5$	4.91[-2]	4.15[-2]	3.56[-2]	3.11[-2]	2.75[-2]	2.46[-2]	2.22[-2]	1.84[-2]	1.57[-2]	1.45[-2]	1.35[-2]	1.18[-2]	$3d_{5/2}4d_{5/2}(5)$

Level	Z=54	Z=56	Z=63	Z=70	Z=73	Z=74	Z=76	Z=79	Z=82	Z=83	Z=90	Z=92	Level-jj
$3d4d\ ^1S_0$	2.96[-3]	2.61[-3]	1.65[-3]	1.05[-3]	8.54[-4]	7.97[-4]	6.92[-4]	5.57[-4]	4.43[-4]	4.11[-4]	2.33[-4]	1.97[-4]	$3d_{3/2}4d_{3/2}(0)$
$3d4d\ ^3P_0$	7.24[-3]	6.39[-3]	4.14[-3]	2.75[-3]	2.32[-3]	2.19[-3]	1.96[-3]	1.66[-3]	1.41[-3]	1.34[-3]	9.28[-4]	8.36[-4]	$3d_{5/2}4d_{5/2}(0)$
$3d4d\ ^1P_1$	9.29[-3]	8.36[-3]	6.00[-3]	4.37[-3]	3.82[-3]	3.65[-3]	3.33[-3]	2.90[-3]	2.51[-3]	2.40[-3]	1.70[-3]	1.54[-3]	$3d_{5/2}4d_{5/2}(1)$
$3d4d\ ^3S_1$	7.35[-3]	6.24[-3]	3.53[-3]	1.98[-3]	1.54[-3]	1.42[-3]	1.20[-3]	9.24[-4]	7.11[-4]	6.51[-4]	3.51[-4]	2.95[-4]	$3d_{5/2}4d_{3/2}(1)$
$3d4d\ ^3P_1$	7.02[-3]	5.97[-3]	3.37[-3]	1.89[-3]	1.47[-3]	1.34[-3]	1.13[-3]	8.68[-4]	6.63[-4]	6.07[-4]	3.26[-4]	2.31[-4]	$3d_{3/2}4d_{3/2}(1)$
$3d4d\ ^3D_1$	8.66[-3]	7.83[-3]	5.58[-3]	4.06[-3]	3.52[-3]	3.35[-3]	3.05[-3]	2.65[-3]	2.27[-3]	2.15[-3]	2.32[-4]	2.35[-4]	$3d_{3/2}4d_{5/2}(1)$
$3d4d\ ^1D_2$	8.87[-3]	7.95[-3]	5.57[-3]	4.00[-3]	3.47[-3]	3.31[-3]	3.02[-3]	2.62[-3]	2.27[-3]	2.15[-3]	2.40[-4]	2.25[-4]	$3d_{3/2}4d_{5/2}(2)$
$3d4d\ ^3P_2$	6.34[-3]	5.40[-3]	3.12[-3]	1.78[-3]	1.39[-3]	1.27[-3]	1.08[-3]	8.32[-4]	6.40[-4]	5.86[-4]	3.12[-4]	2.60[-4]	$3d_{5/2}4d_{3/2}(2)$
$3d4d\ ^3D_2$	8.45[-3]	7.58[-3]	5.34[-3]	3.85[-3]	3.35[-3]	3.20[-3]	2.92[-3]	2.54[-3]	2.21[-3]	2.11[-3]	1.51[-3]	1.37[-3]	$3d_{5/2}4d_{5/2}(2)$
$3d4d\ ^3F_2$	6.03[-3]	5.16[-3]	2.98[-3]	1.70[-3]	1.33[-3]	1.22[-3]	1.03[-3]	7.97[-4]	6.14[-4]	5.63[-4]	3.30[-4]	2.57[-4]	$3d_{3/2}4d_{3/2}(2)$
$3d4d\ ^1F_3$	6.39[-3]	5.47[-3]	3.14[-3]	1.78[-3]	1.39[-3]	1.27[-3]	1.07[-3]	8.26[-4]	6.32[-4]	5.78[-4]	3.02[-4]	2.50[-4]	$3d_{3/2}4d_{3/2}(3)$
$3d4d\ ^3D_3$	6.21[-3]	5.28[-3]	3.03[-3]	1.71[-3]	1.33[-3]	1.23[-3]	1.03[-3]	7.97[-4]	6.11[-4]	5.59[-4]	2.94[-4]	2.43[-4]	$3d_{5/2}4d_{3/2}(3)$
$3d4d\ ^3F_3$	8.75[-3]	7.84[-3]	5.50[-3]	3.95[-3]	3.43[-3]	3.28[-3]	2.99[-3]	2.60[-3]	2.26[-3]	2.16[-3]	1.54[-3]	1.40[-3]	$3d_{3/2}4d_{5/2}(3)$
$3d4d\ ^3G_3$	8.88[-3]	7.97[-3]	5.62[-3]	4.04[-3]	3.52[-3]	3.36[-3]	3.06[-3]	2.66[-3]	2.31[-3]	2.20[-3]	1.57[-3]	1.43[-3]	$3d_{5/2}4d_{5/2}(3)$
$3d4d\ ^1G_4$	9.19[-3]	8.24[-3]	5.77[-3]	4.12[-3]	3.58[-3]	3.42[-3]	3.11[-3]	2.70[-3]	2.34[-3]	2.24[-3]	1.60[-3]	1.45[-3]	$3d_{3/2}4d_{5/2}(4)$
$3d4d\ ^3F_4$	8.74[-3]	7.81[-3]	5.48[-3]	3.92[-3]	3.41[-3]	3.26[-3]	2.97[-3]	2.58[-3]	2.24[-3]	2.14[-3]	1.53[-3]	1.39[-3]	$3d_{5/2}4d_{5/2}(4)$
$3d4d\ ^3G_4$	6.45[-3]	5.48[-3]	3.17[-3]	1.79[-3]	1.39[-3]	1.28[-3]	1.08[-3]	8.31[-4]	6.36[-4]	5.81[-4]	3.04[-4]	2.52[-4]	$3d_{5/2}4d_{3/2}(4)$
$3d4d\ ^3G_5$	9.34[-3]	8.33[-3]	5.83[-3]	4.17[-3]	3.62[-3]	3.46[-3]	3.15[-3]	2.73[-3]	2.37[-3]	2.26[-3]	1.61[-3]	1.46[-3]	$3d_{5/2}4d_{5/2}(5)$

[32] Y. Skobelev, V. M. Dyakin, A. Y. Faenov, A. Bartnik, and H. Fiedorowicz, J. Phys. B **32**, 113 (1999).
[33] C. Z. Dong, S. Fritzsche, and L. Y. Xie, J. Quant. Spectr. Rad. Transf. **76**, 447 (2003).
[34] J. Y. Zhong, J. Zhang, J. L. Zeng, G. Zhao, and M. F. Gu, At. Data Nucl. Data Tabl. **89**, 101 (2005).
[35] J.-F. Wyart and A. N. Ryabtsev, Phys. Scr. **33**, 215 (1986).
[36] S. S. Churilov, A. N. Ryabtsev, and J.-F. Wyart, Phys. Scr. **38**, 326 (1988).
[37] B. J. MacGowan, S. Maxon, P. L. Hagelstein, C. J. Keane, R. A. London, D. L. Matthews, M. D. Rosen, J. H. Scofield, and D. A. Whelan, Phys. Rev. Lett. **59**, 2157 (1987).
[38] B. J. MacGowan, S. Maxon, L. B. Da Silva, D. J. Fields, C. J. Keane, D. L. Matthews, A. L. Osterheld, J. H. Scofield, G. Shimkaveg, and G. F. Stone, Phys. Rev. Lett. **65**, 420 (1990).
[39] B. J. MacGowan, L. B. Da Silva, D. J. Fields, R. F. A, C. J. Keane, J. A. Koch, D. L. Matthews, S. Maxon, A. L. Osterheld, J. H. Scofield, et al., Proc. 2nd Intern. Colloq. p. 221 (1990).
[40] A. Rahman, E. C. Hammarsten, S. Sakadzic, J. J. Rocca, and J.-F. Wyart, Phys. Scr. **67**, 414 (2003).
[41] A. Rahman, J. J. Rocca, and J.-F. Wyart, Phys. Scr. **70**, 21 (2004).

[42] S. S. Churilov, A. N. Ryabtsev, and J.-F. Wyart, Phys. Scr. **71**, 457 (2005).
[43] E. Träbert, P. Beiersdorfer, K. B. Fournier, S. B. Utter, and K. L. Wong, Can. J. Phys. **79**, 153 (2001).
[44] S. B. Utter, P. Beiersdorfer, and E. Träbert, Can. J. Phys. **80**, 1503 (2002).
[45] U. I. Safronova, W. R. Johnson, M. S. Safronova, and A. Derevianko, Phys. Scr. **59**, 286 (1999).
[46] U. I. Safronova, A. Derevianko, M. S. Safronova, and W. R. Johnson, J. Phys. B **32**, 3527 (1999).
[47] U. I. Safronova, T. E. Cowan, and M. S. Safronova, J. Phys. B **38**, 2741 (2005).
[48] M. H. Chen, K. T. Cheng, and W. R. Johnson, Phys. Rev. A **47**, 3692 (1993).
[49] Yu. Ralchenko, F.-C. Jou, D.E. Kelleher, A.E. Kramida, A. Musgrove, J. Reader, W.L. Wiese, and K. Olsen (2005). NIST Atomic Spectra Database (version 3.0.2), [Online]. Available: http://physics.nist.gov/asd3 [2006, January 4]. National Institute of Standards and Technology, Gaithersburg, MD.
[50] URL http://das101.isan.troitsk.ru/cowan.htm.
[51] W. R. Johnson, S. A. Blundell, and J. Sapirstein, Phys. Rev. A **37**, 307 (1988).